Chapter 2

Influences of Doping on Photocatalytic Properties of TiO_2 Photocatalyst

Fei Huang, Aihua Yan and Hui Zhao

Additional information is available at the end of the chapter

http://dx.doi.org/10.5772/63234

Abstract

As a kind of highly effective, low-cost, and stable photocatalysts, TiO_2 has received substantial public and scientific attention. However, it can only be activated under ultraviolet light irradiation due to its wide bandgap, high recombination, and weak separation efficiency of carriers. Doping is an effective method to extend the light absorption to the visible light region. In this chapter, we will address the importance of doping, different doping modes, preparation method, and photocatalytic mechanism in TiO_2 photocatalysts. Thereafter, we will concentrate on Ti^{3+} self-doping, nonmetal doping, metal doping, and codoping. Examples of progress can be given for each one of these four doping modes. The influencing factors of preparation method and doping modes on photocatalytic performance (spectrum response, carrier transport, interfacial electron transfer reaction, surface active sites, etc.) are summed up. The main objective is to study the photocatalytic processes, to elucidate the mechanistic models for a better understanding the photocatalytic reactions, and to find a method of enhancing photocatalytic activities.

Keywords: TiO_2, doping, photocatalytic properties, mechanism, carrier transfer

1. Background

As the best known photocatalyst, TiO_2 has attracted more attention and interest of many researchers due to its exceptional properties, such as high refractive index and ultraviolet (UV) absorption, excellent incident photoelectric conversion efficiency and dielectric constant, good photocatalytic activity, photostability, chemical stability, and long-time corrosion resistance as well as nontoxicity [1–4]. It has been widely used to solve a variety of environmental problems for the water-based solution utilization.

However, there are three key drawbacks for TiO_2 materials to limit their practical application. Firstly, one shortcoming is related to their large bandgap (3.0 eV for rutile and 3.2 eV for anatase TiO_2, respectively). It is well known that the photon absorption of semiconductors depends greatly on their bandgap energy. The photons can only be absorbed by the photocatalyst if the photon energies are higher than the semiconducting bandgap energy. Consequently, its surface photoactivation can be exclusively done under UV radiation ($\lambda \leq 390$ nm) or it only can respond and generate electron-hole pairs under UV light [5]. However, solar light consists of 5% UV light (300–400 nm), 43% visible light (400–700 nm), and 52% infrared light (700–2500 nm). That is, the UV light only occupies a small portion of the sunlight and a large part of solar energy cannot be utilized. In the future, one of the most urgent tasks is finding or modifying the photocatalysts with proper semiconducting bandgaps to maximize the absorption of solar energy. Secondly, a high recombination rate of electron-hole pairs is another disadvantageous effect on the photocatalytic efficiency for TiO_2 photocatalysis, resulting in a low quantum yield rate and a limited photooxidation rate. Thirdly, the weak separation efficiency of photocarries results in low photocatalytic activity. All three limitations induce great influence for a wide practical application.

To overcome above-mentioned problems, many studies have been conducted in the past 5 years based on the idea of extending the wavelength range of the photoactivation of TiO_2 photocatalysts towards visible light region and enhancing the utilization efficiency of solar energy. That is, an increased amount of energy from the solar light spectrum is well utilized.

Recently, a path to achieve above-mentioned goal is represented by alien ion doping to improve the adsorption capacity and photocatalytic activity, such as self-doping [6–8], nonmetal doping [9–11], transitional metal doping [12, 13], and rare-earth metal doping [14, 15]. Usually, the doped ions introduce additional energy levels into the band structure, which can be used to trap electrons or holes to separate carriers from the bands, thus allowing more carriers to successfully diffuse to the surface. It has also been suggested that the required red shift of the absorption edge might be done by increasing the impurity ion concentration or increasing the oxygen defects in TiO_2. That is, the purpose of doping is relatively straightforward: modifying its large bandgap and electronic structure to optimize its optical properties for visible light harvest, improving each step in the charge kinetics to reduce the massive recombination of photogenerated carriers, and improving the interface and surface characteristics [16]. On the contrary, the photocatalytic activity depends strongly on the exposed crystalline faces [17, 18]. Given that different crystal surfaces have different surface energy levels for the conduction band (CB) and valence band (VB), such differences in the energy levels will drive the electrons and holes to different crystal faces. Obviously, doping can effectively modulate the lattice face structures.

To make clear the original question about the photocatalytic mechanism for doped TiO_2, it is important to explain and understand the doping process, doping method, and defect chemistry, especially the physics of the energy levels induced by the incorporation of dopants. This chapter comprises the following four sections to elaborate above concerns and recent progresses:

1. Ti^{3+} self-doping in TiO_2 crystals and its photocatalytic mechanism,

2. Nonmetal doping in TiO_2 crystals and its photocatalytic mechanism,
3. Metal doping in TiO_2 crystals and its photocatalytic mechanism, and
4. Codoping in TiO_2 crystals and its photocatalytic mechanism.

2. Self-doping

It is widely accepted that the degradation of pollutants in water proceeds by oxidation either reacting directly with generated holes or indirectly with OH free radicals [19, 20]. Moreover, the photocatalytic activity of TiO_2 is often dependent on the nature and density of surface defect sites. Usually, incorporating dopants into TiO_2 crystals at the oxygen (O) and/or titanium (Ti) sites can generate midgap states [21]. Furthermore, interactions of photogenerated carriers with impurities in TiO_2 can also alter the electric structure and energy band structure, which enhances the photocatalytic performance [22]. Of course, excess doping also increases crystal defects (for example, oxygen vacancies, titanium vacancies, and interstitial titanium), thermal instability, carrier trapping, and carrier recombination centers [23, 24]. In other words, system-charge equilibria and/or geometric structure optimization should be considered during the doping process, especially the doping level or doping concentration and dopant distribution.

Recently, both experimental results and theoretical predictions have demonstrated that Ti^{3+} self-doped TiO_2 could obviously increase concomitant intrinsic oxygen vacancies in TiO_2 crystals because the surface chemistry of nonstoichiometric TiO_2 containing Ti^{3+} differs markedly from that of perfect TiO_2. Different from traditional impurity incorporation, Ti^{3+} self-doping has been reported as an effective way to extend the visible light absorption of TiO_2, which can avoid the mismatching of atomic diameters with other foreign elements [25–28]. Self-doping can easily modulate and realize the system-charge equilibria just through synthesis method, process control, and raw material selection. Theoretical calculations evidence that interstitial Ti can cause impurity energy levels at 1.23 to 1.56 eV below the CB, whereas vacant Ti just makes impurity energy levels above the VB [29, 30]. Usually, the two defects can result in extra shoulder absorption or a tail absorption, which is the root cause for the enhancement of photocatalytic performance [31, 32].

2.1. Preparation of Ti^{3+} self-doping

The basic process of self-doping includes that the electrons can be trapped and tended to reduce Ti^{4+} cations to Ti^{3+} state [33], the holes oxidize O^{2-} anions for the formation of O^- trapped hole or even O_2 gas, and the charge transfer steps are as follows:

$$TiO_2 + h\nu \rightarrow e^-_{CB} + h^+_{VB} \tag{1}$$

$$e^-_{CB} + Ti^{4+} \rightarrow Ti^{3+}\left(trapped\ electron\right) \tag{2}$$

$$h^{+}_{VB} + O^{2-} \rightarrow O^{-}(trapped\ hole) \tag{3}$$

$$4h^{+}_{VB} + 2O^{2-} \rightarrow O_2 \tag{4}$$

Subsequently, many methods are developed according to the above mechanism, such as hydrothermal method [25, 34–37], solvothermal method [38, 39], metallic reduction method [28, 40], solution-based oxidative method [41, 42], solution-based reduction method [43, 44], ionothermal method [26], vapor-fed aerosol flame synthesis [27], combustion method [33], and evaporation-induced self-assembly (EISA) method [45].

The hydrothermal method is widely used to synthesize Ti^{3+} self-doped TiO_2 compared to other methods. Wang et al. changed hydrothermal conditions to treat a gel precursor and obtained Ti^{3+} self-doped TiO_2 nanoparticles [34]. They found that the contents of Ti^{3+} and oxygen vacancy (O_v) in TiO_2 crystals could be reasonably adjusted. Xin et al. demonstrated that the oxidation-based solvothermal synthesis of Ti^{3+} self-doped anatase TiO_2 was an effective strategy to prepare uniform Ti^{3+} self-doped anatase TiO_2 nanocrystals. Both the concentration and location of the Ti^{3+} defects could be well managed by simply controlling the annealing temperature. This temperature-mediated management of the location and concentration of Ti^{3+} defects was achieved through a Ti^{3+} reversible diffusion mechanism [38]. The metallic reduction method was also used to synthesize Ti^{3+} self-doped TiO_2 with dominant (001) facets, and the presence of Zn obviously caused the formation of Ti^{3+} ions coming from the reduction of Ti^{4+} [40].

Liu et al. successfully synthesized anatase Ti^{3+} self-doped TiO_{2-x} nanoparticles by a simple interface ion diffusion-redox reaction, and the resulting Ti^{3+} self-doped TiO_{2-x} had high crystallinity and showed enhanced visible light-driven photocatalytic oxidation [41]. Tian et al. used $NaBH_4$ as a reduced source and prepared TiO_2 nanobelts, and the theoretical calculations and experimental results indicated that the oxygen vacancies and Ti^{3+} ions were successfully formed by reduction [43].

2.2. Mechanism of enhanced photocatalytic

It is well known that the Fermi level is much closer to the CB tail at a high oxygen vacancy concentration. Therefore, it is reasonably deduced that the higher oxygen vacancies can lead to an enhanced absorption of photon energy below the direct bandgap. The midgap states below the CB edge turn broad at an enhanced oxygen vacancy concentration (**Figure 1**). Meanwhile, the band of defect states resulting from oxygen vacancies is close to the CB edge, allowing photogenerated electrons to easily exchange between two bands. Namely, the electrons from the VB can easily transfer to the oxygen vacancy level under visible light irradiation. In other words, the electron transfer takes place from both VB and oxygen vacancy level localized states to the tailed CB. Consequently, the onset of optical absorption of the TiO_2 nanocrystals is lowered to 900 to 1100 nm [46–48].

http://dx.doi.org/10.5772/63234

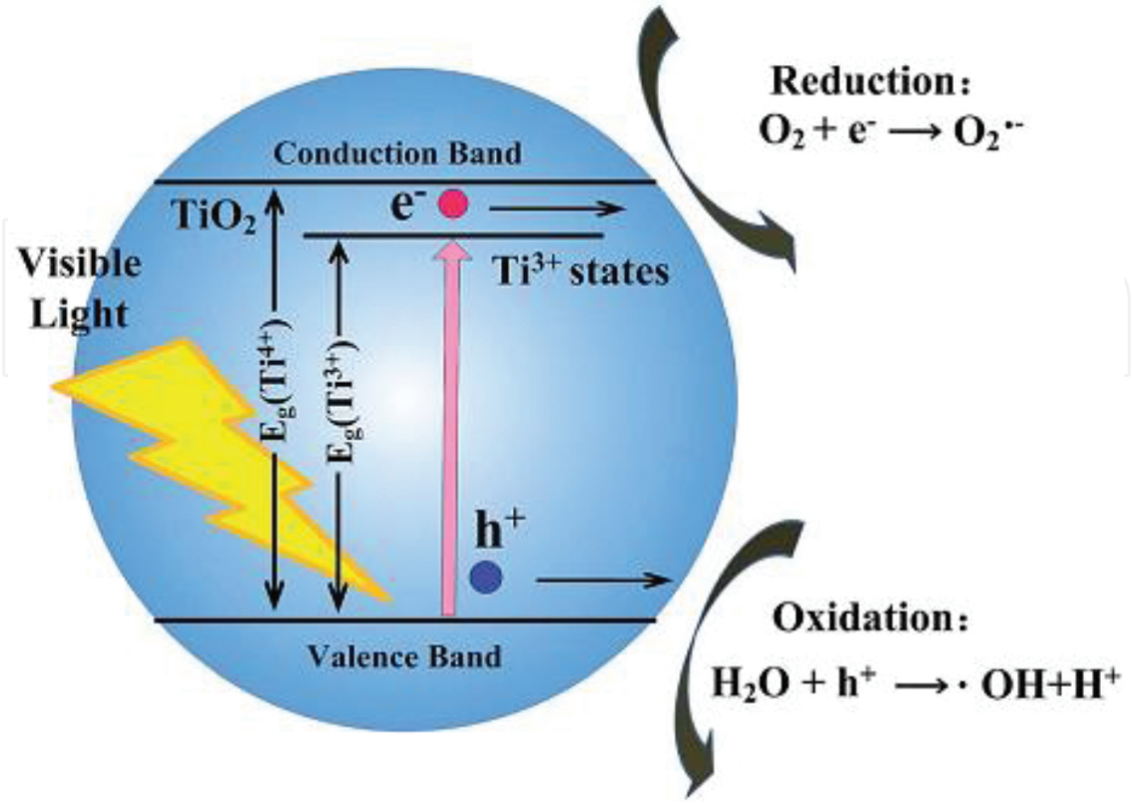

Figure 1. Schematic diagram of a proposed photocatalytic mechanism of Ti^{3+} self-doped TiO_2 for the visible-light response [27].

Many theoretical data from calculation and simulation also confirm that the local electrostatic balance is broken when host Ti^{4+} ions are reduced to Ti^{3+} ions, and oxygen vacancies are introduced because of charge compensation [49–51]. Because the effective charge of the oxygen vacancy is positive, the central Ti^{3+} is expected to shift away from the oxygen vacancy, forming a special sublevel electric state. Conversely, the shift Ti^{3+} also forces the four O^{2-} ions to move towards the oxygen vacancy to keep the electrostatic balance. The electrons can be photoexcited to CB under the irradiation of visible light. Meanwhile, the oxygen vacancies can inhibit the photogenerated electron-hole recombination. Furthermore, those Ti^{3+} ions act as hole traps and suppress the recombination of carriers and therefore extend the lifetime of the charges. That is, the higher light absorption in Ti^{3+} self-doping may come from the strong distortion of the outer orbitals of the Ti^{3+} ions.

In other words, Ti^{3+} self-doped TiO_2 exhibits a remarkable activity and enhanced performance as a photocatalyst. However, it is difficult to implant Ti^{3+} into TiO_2 crystals in practical application because Ti^{3+} species are usually unstable and can be easily oxidized by O. Therefore, it is still challenging to develop a simple and phase-controlled method to synthesize stable Ti^{3+} self-doped TiO_2 photocatalysts in the future. Moreover, it is important to have a comprehensive understanding of the methods and the techniques of Ti^{3+} generation and monitoring as well as Ti^{3+} property exploration.

3. Nonmetal doping

Nonmetal elements with high ionization energies and high electronegativity, such as nitrogen (N) [52–54], carbon (C) [55, 56], boron (B) [57–59], sulfur (S) [60, 61], fluorine (F) [62–64], and chlorine (Cl) [65, 66], are an efficient strategy to enhance the visible light photocatalytic activity, which results in higher photocatalytic activity in the visible light region owing to the bandgap narrowing and the shift of absorption edge.

The basic process is that the nonmetal dopants influence the VB through interaction with the O 2*p* electrons. The localized states or *p* states of nonmetallic dopants generally form the impurity levels and lie above VB, which extends the optical absorption edge of TiO_2. On the contrary, nonmetal dopants within a surface can exist as isolated atoms rather than clusters. Consequently, the distribution of dopant states is above the VB maximum, which has greater potential for realizing visible light photoactivity.

3.1. N doping

Among all nonmetal elements, N element has been proven to be one of the most efficient dopants for visible light-responsive TiO_2 photocatalyst. Since Asahi et al. made a breakthrough work in 2001 and found that doped TiO_2 with N could enhance its photocatalytic activity for the photodegradation of methylene blue under visible light irradiation [67]. Many theoretical calculations and experiments have demonstrated and confirmed that N is one of the most promising dopant candidates for red shift of the absorption edge so far. Some authors suggested a model in which the incorporation of N via O substitution results in bandgap narrowing due to the mixing of the N 2*p* and O 2*p* states, which shows a remarkable red shift of the spectrum onset [68, 69]. In most of the reported studies, only N dopant concentration below 1 at.% are mentioned, and surface photoactivation with visible light is less effective compared to UV [70–72]. In other words, N-doped TiO_2 is a promising candidate photocatalyst for enhanced light harvest in the visible region because it has strongly localized N 2*p* states (0.3–0.5 eV) at the VB maximum [73].

3.1.1. Preparation

The formation mechanism of N-doped catalysts obtained via different preparation methods is usually different. Moreover, N doping plays an important role on the exposed high-energy facets to a certain extent, which is apparently influenced by different preparation methods.

Generally speaking, there are two kinds of processes to prepare N-doped TiO_2. One process can be ascribed as one-step direct incorporation of N atoms into TiO_2 lattice, such as sol-gel method [74–76], chemical vapor deposition (CVD) [77, 78], atomic layer deposition (ALD) [79–81], hydrothermal method [82–84], solvothermal method [85–88], sol-hydrothermal process [89], hydrolysis-precipitation process [90], bioprocess-inspired method [91], electrochemical method [92–94], ion implantation [95, 96], combustion method [97–99], mechanochemical method [100, 101], low-temperature direct nitridization method [102], and microwave-assisted method [103].

Samsudin et al. synthesized undoped and N-doped TiO_2 via a sol-gel technique using Ti(IV) isopropoxide and triethylamine as the Ti and N precursors, respectively [74]. N was doped interstitially forming Ti-O-N or Ti-N-O linkages, and induced local states 0.23 to 0.26 eV above the VB, which was responsible for the visible light response between 400 and 550 nm. Gao et al. prepared N-doped TiO_2 films by the dielectric barrier discharge enhanced CVD method using Ti tetraisopropoxide and NH_3 as Ti precursor and doping gas [77]. It was found that N doping sources changed the growth orientation, affected the surface microstructure, narrowed the bandgap, and improved the photocatalytic activity in the visible light region. Liu et al. conducted an ALD method to fabricate N-doped TiO_2 hollow fibers with polysulfone fibers as a template [79]. The results showed that N was successfully inserted into the anatase TiO_2 lattice to form impurity levels above the VB top that narrowed the bandgap.

Therein, the hydrothermal method and solvothermal method are most frequently used because of their low cost, perfect crystallinity, and good repeativity. Wang et al. prepared N-doped TiO_2 nanoparticles by a facile one-pot hydrothermal treatment in the presence of L-lysine, and the results showed that N-TiO_2/C nanocomposites increased absorption in the visible light region and exhibited a higher photocatalytic activity than pure TiO_2, commercial P25, and previously reported N-doped TiO_2 photocatalysts [82]. Li et al. prepared a series of N-doped anatase TiO_2 samples using a solvothermal method in an organic amine/ethanol-water reaction system [85]. Both the degree of N doping and oxygen vacancies made contributions to the visible light absorption of the sample.

Recently, Cheng et al. synthesized N-doped TiO_2 nanoparticles through a hydrolysis-precipitation process using ammonia water as the doping species [90]. They found that the light absorbance edge of N-doped TiO_2 nanoparticle was obviously red-shifted to visible light region and the separation rates of photogenerated carriers were greatly improved. Further analysis implied that the VB maximum of O 2*p* was 2.3 eV. Hu et al. also developed a facile low-temperature direct nitridization method to synthesize colloidal N-doped TiO_2 nanocrystals in triethylamine solution during the hydrolysis of tetrabutyl titanate followed by acidic peptization at 70°C [102]. The N-doped TiO_2 exhibited higher photocatalytic activity both in the UV and visible light regions in contrast to the undoped TiO_2 because of the improved light response in the range of 400 to 500 nm, narrowing bandgap, more production of e^--h^+ pairs, and inhibiting recombination of the photo-induced carriers.

The other important preparation process of N-doped TiO_2 can be ascribed as two-step oxidization of Ti nitride, such as sputtering method [104, 105], thermal annealing [106–108], and plasma-enhanced microarc oxidation [109]. As for two-step methods, there are less research compared to one-step methods due to its higher cost and more complex technique process. Abadias et al. thought that the visible light activity of these materials mainly depended on the location of this impurity states and the microstructure of the N-doped TiO_2 materials [104]. They synthesized N-TiO_2 films through reactive magnetron sputtering method under a mixture gas of argon (Ar), N, and O. N diffusion was suggested to be responsible for the more complex crystallization and a better photocatalytic activity. Ha et al. prepared a new type of N-doped TiO_2 mesoporous inverse opal structure via heat treatment in the presence of an N-rich precursor, and the N doping with 9.4 wt.% concentration narrowed the bandgap from 3.2

to 2.4 eV, which corresponded to light absorption at wavelengths as long as 520 nm [106]. Jiang et al. developed a novel plasma-enhanced microarc oxidation process for preparing a high concentration substitutional N-doped TiO_2, compared to the traditional thermal annealing, and the process provides a possibility to increase the N doping concentration up to 3.21 at.% in $TiO_{2-x}N_x$, which exhibits a significant red shift in the bandgap transition and narrows bandgap to 2.6 eV [109].

3.1.2. Photocatalytic mechanism of N-doped TiO_2

The mechanism, especially the origin of visible light photoactivity for N-doped TiO_2, is still in debate up to now. Valentin et al. [111] and Gao et al. [101] studied substitutional and interstitial N impurities in bulk anatase TiO_2 lattice (**Figure 2**). They thought that the N atom replaced lattice O in TiO_2 for the substitutional case and showed positive oxidation state ranging from hyponitrite species (NO^-), nitrite (NO_2^-), to nitrate species (NO_3^-). The visible light responses for substitutional N-doped anatase TiO_2 came from occupied N 2*p* localized states, which were slightly above the VB maximum. The N-O bond showed localized π-bond states. The two bonding states were found in deep energy level and lay below the top of the O 2*p* band. The other two antibonding states were found located over the O 2*p* band. In other words, the localized states were responsible for the excellent optical adsorption when the N atom was located at the substitutional site. On the contrary, interstitial site for N doping had some disadvantageous effects on the photocatalytic reaction because of the hole trapping.

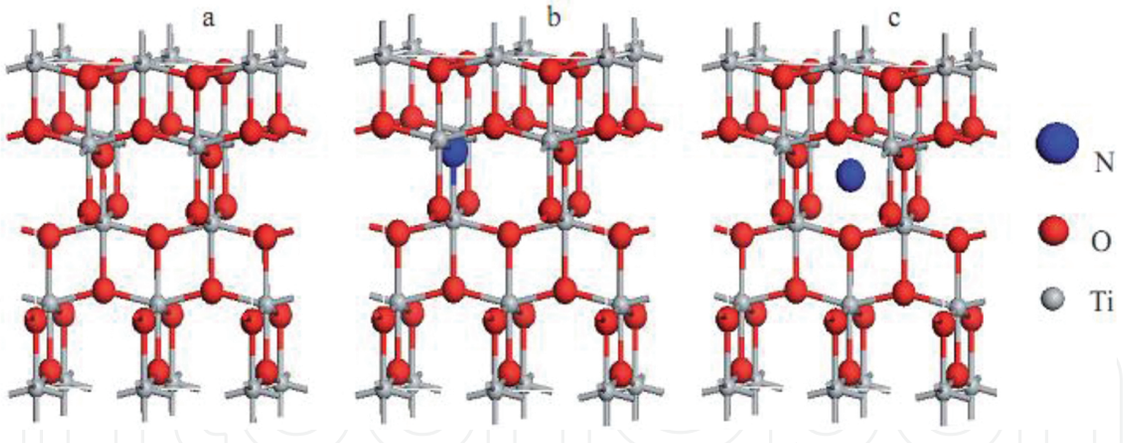

Figure 2. Supercells of (a) pure, (b) substitutional, and (c) interstitial TiO_2 [111].

Energy bandgap models also predict that substitutional (interstitial) N generates shallow (deep) midgap states above the top of the VB due to the mixing of N 2*p* and Ti 3*d* orbitals (**Figure 3**). Usually, N doping is associated with the formation of oxygen vacancies and electrons to maintain lattice neutrality. From this perspective, it has been suggested that the presence of extra oxygen vacancies might be the key factor allowing for better photocatalytic performances to be achieved, which causes a red shift of the absorption band edge due to a positive shift of VB and improves electron injection [112–114]. Under visible light irradiation, electrons of the localized N 2*p* states can be excited up to the individual CB, leaving holes on

the localized states. The energy barrier between midgap states would suppress electron transfer. This can also inhibit the recombination of photoelectrons and holes to some extent [115]. In other words, the efficient separation of photo-induced carriers under visible light excitations enables N-doped TiO_2 to have higher photocatalytic activity in a wide wavelength ranging from UV to the visible region.

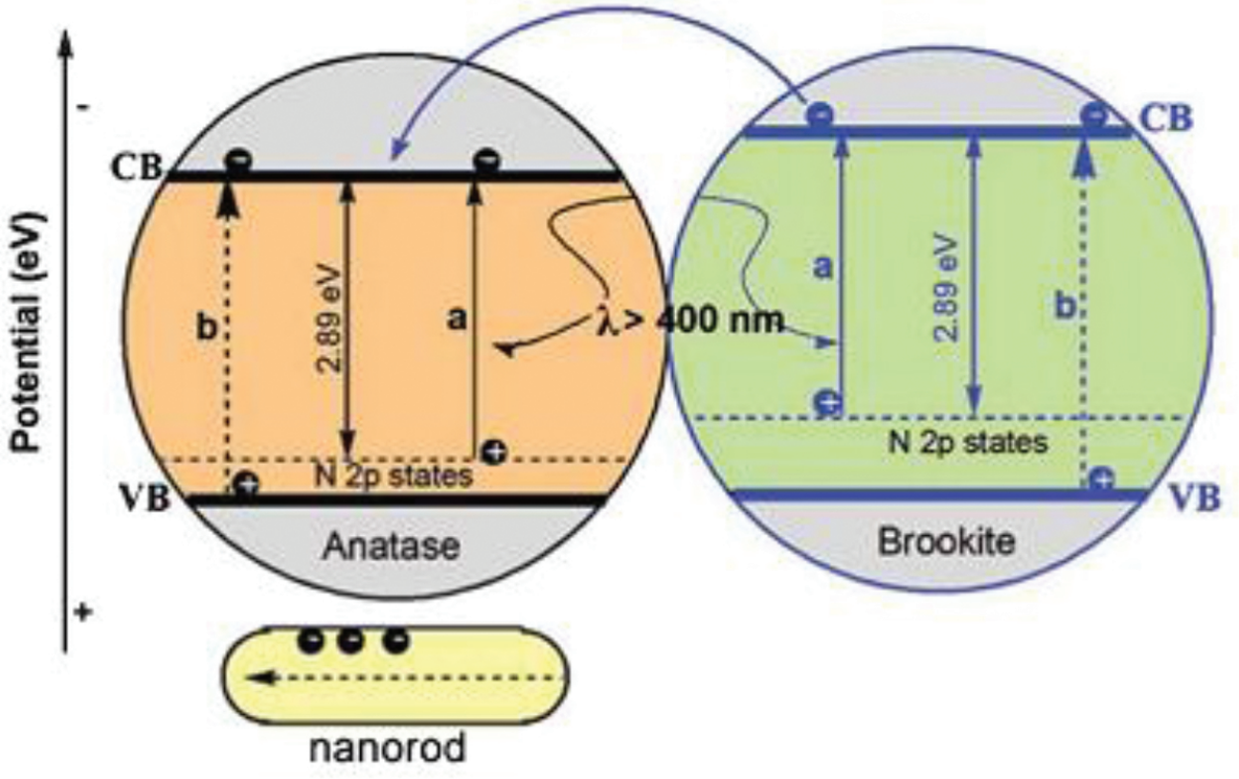

Figure 3. Schematic illustration of electron migration in anatase/brookite structures: under visible light irradiation (path a) and under UV light illumination (path b) [114].

3.2. C doping

Among the nonmetal elements, C doping has also been proposed as one of the best candidates [116]. The origin of C doping is mainly incorporated interstitially, narrowed bandgap and resulted in a red shift in the UV-visible (UV-vis) spectrum, resulting in an increase in adsorption of near-infrared (NIR) spectrum [117, 118]. Khan et al. first reported that C-doped TiO_2 was visible light active, and found that that the three kinds of C species could influence the photocatalytic activity, namely, elemental C, carbonate species (C-O bond) as interstitial dopant, and C substituted for O (Ti-C bond) in TiO_2 lattice [119].

Subsequently, a lot of researches were conducted to synthesize C-doped TiO_2 photocatalysts [120–124]. Shi et al. prepared nanometer-sized C-doped TiO_2 nanoplates with exposed {001} facets via the hydrothermal treatment of TiC powder in an HF-HNO_3 mixed aqueous solution and found that C doping also obviously presented red shift absorption edge towards visible

light [120]. Further analysis found that the electrons in the localized C states could be excited to the CB under visible light irradiation and effectively scavenged by molecular O to produce the superoxide radical anion ($\bullet O_2^-$) and hydrogen peroxide (H_2O_2), which could interact to produce hydroxyl radicals (•OH). Recently, Shao et al. prepared amorphous C-doped TiO_2 with visible light photocatalytic activity by a facile sol-gel route for the first time. The results also indicated that the most active sample with oxygenic groups had a narrower bandgap and lower recombination of electron hole, significantly broadening its potential for many practical applications [122].

About the mechanism of photocatalytic activity for C-doped TiO_2 catalysts, it is similar to N-doped TiO_2 catalysts, except some little differences. Liu et al. investigated that C doping in the TiO_2 lattice had graphite- and carbonate-like species at interstitial positions [125]. They thought that the two C states could narrow the bandgap of anatase TiO_2, serving as a photosensitizer to absorb visible light and promote the charge carrier separation, which enhanced the visible light photocatalytic activity remarkably. Zhang et al. insisted that the substitutional C (C_s) at O sites modified the electronic band structure of TiO_2 by mixing C 2*p* orbitals with O 2*p* orbitals, resulting in bandgap narrowing [123]. Under visible light irradiation, electrons can be excited directly into the CB and transferred to the adsorbed O molecule to produce $\bullet O_2^-$ and subsequently •OH with strong oxidation power. Recently, Sun and Zhang investigated the C doping of anatase TiO_2 in detail using density functional theory (DFT) calculation [126]. They found that C_{Ti} and C_i with a shallow donor had no effect on the bandgap, whereas the $(CO)_{2O}$, C_O-V_O, and $(C_2)_{2O}$ defect reduced the bandgap to about 1.1, 1.7, and 1.4 eV, respectively. Based on the electronic structure analysis of the C defects, they excluded the possibility of C occupying Ti sites or interstitial sites to be responsible for the enhancement of photoactivity in the visible light region.

3.3. S doping

S doping in TiO_2 structure also shows bandgap narrowing effects [127]. However, its large ionic radius makes it difficult to incorporate into TiO_2 crystals due to the large formation energy. Therefore, the key issues are to find a facile, low-cost, and stable process to synthesize S-doped TiO_2.

Goswami and Ganguli developed a novel approach to synthesize sulfated TiO_2 nanoparticles using 15% Ti trichloride and thiophene in the presence and absence of oxalic acid [128]. They found that S-doped samples had higher surface area, smaller crystallite size, greater thermal stability, and better photocatalytic performance. Li et al. demonstrated a facile nonhydrolytic thermolysis route for monodisperse S-doped TiO_2 nanocatalysts in hot boiling organic solvents of oleic/oleyl-amine/1-octadecene [129]. Compared to the undoped TiO_2 nanocatalysts, S-doped TiO_2 nanocatalysts presented obviously enhanced visible light activation for the degradation of rhodamine B and methylene blue dyes under the artificial visible light irradiation. Recently, Ramacharyulu et al. synthesized S-doped TiO_2 catalysts by a sol-gel process followed by hydrothermal treatment at low temperature and tested for catalytic activity by natural sunlight photocatalytic degradation of a toxic chemical warfare agent [130]. It was observed that S-doped TiO_2 exhibited superior photocatalytic activity under sunlight irradia-

tion. Further analysis indicated that the superior photocatalytic activity could be attributed to the presence of S^{4+}/S^{6+} or N^- impurity levels. Lin et al. [131] and Sharotri and Sud [131, 132] further found the importance of S^{6+} for S-doped TiO_2 photocatalysts, which could form h^+/e^- trapping centers, delay the phase transition from anatase to rutile, promote photocatalytic activity, and prevent h^+/e^- recombination.

3.4. Halogen doping

Halogen doping in TiO_2 crystals is another important approach to improve photocatalytic performance, such as F doping [133–135], Cl doping [136–138], and iodine (I) doping [139–141]. Pan et al. developed an effective bottom-up synthesis strategy to prepare monodisperse F-doped TiO_2 mesoporous spheres by integrating sol-gel and solvothermal processes [133]. The photocatalytic experiments showed that the formation of surface fluorination was helpful to improve and enhance light harvesting in the UV-vis range. Fang et al. also synthesized F-doped rutile TiO_2 with tunable solar absorption via one-pot hydrothermal method [142]. They found that the optical bandgap of the catalyst could be easily manipulated from 3.05 to 2.58 eV through altering the initial F:Ti molar ratio.

The origin of the visible light activity of F-doped TiO_2 has been systematically investigated by many researchers via comprehensive theoretical and experimental studies [134, 143–145]. It is widely accepted that the three-coordinated surface F atoms with higher 1s binding energy are identified to be the origin of the visible light activity. The surface group can also trap the CB electrons by tightly holding electrons due to the strongest electronegativity of F. The calculated results using DFT principle show that F implantation resulted in Ti^{3+} self-doping and contributes to the enhancement photocatalytic activity. Moreover, the strong electron-withdrawing ability of the surface three-coordinated surface F also reduces the recombination of photogenerated electrons and holes.

Similarly, Cl doping has the same role in TiO_2 crystals with F doping. Wang et al. prepared Cl-doped TiO_2 nanocrystalline via a simple single-step method by sonicating a solution of tetraisopropyl titanate and sodium chloride in water/ethanol at 70°C and found that the Cl doping of TiO_2 shifts the absorption edge toward a higher wavelength [136]. The photodegradation rates of butyl benzyl phthalate reached 92% under visible light irradiation for 240 min, which was much higher than undoped TiO_2.

Doping with I element in TiO_2 crystals also can enhance light absorption and decrease recombination [146–149]. Lin et al. synthesized I-modified TiO_2 nanocrystallites through a combination of sol-gel process and solvothermal process in the presence of HI solution [146]. The results showed that the I in the form of I_2 was responsible for the visible light response. Liu et al. developed a new strategy for homogeneous doping of I molecules (I_2) to achieve bandgap narrowing of TiO_2 nanosheets and investigated the extension of the intrinsic absorption edge into the visible light region through a shifting of the VB maximum [149]. Importantly, the geometric structure of the host retained its integrity. The experiment together with first-principles calculations revealed the molecular nature of adsorbed I atoms and implied that the mechanism of electronic structure modulation in the TiO_2 layers changed depending on the concentration of I_2 molecules.

3.5. Other doping

B^{3+} is incorporated both substitutionally and interstitially in TiO_2 crystals. Usually, the replacement of B^{3+} for Ti^{4+} generates one hole in O 2*p* orbital, which can also be accompanied by a blue shift of the UV-vis absorption spectrum and an increase in oxygen vacancies [150, 151]. Xu et al. developed a new method allowing a clean one-step synthesis to obtain B-doped TiO_2 for the first time [150]. B doping resulted in a shift of the absorption edge up to 460 nm with a concomitant reduction of the bandgap energy. The narrowing bands were attributed to ionized oxygen vacancies and defect states in anatase for the presence of interstitial B tricoordinate and tetracoordinate to O.

Another concerned nonmetal dopant is phosphorus (P). Many papers indicated that P dopant could also improve the photocatalytic activity [152, 153]. Zheng et al. synthesized a novel thermally stable P-doped TiO_2 by liquid hydrolysis of $TiCl_4$ using hypophosphorus acid as the precursor of the dopant [152]. They found that increased surface P content led to a linear enhancement of the specific adsorption capacity of methylene blue because of the Coulombic attractive force between the cationic dye and the negatively charged P-doped TiO_2 surface.

4. Metal dopants

It is well known that the photoexcitation of TiO_2 catalysts involves excitation, diffusion, and surface transfer of photogenerated carriers. Therefore, the carrier's lifetime is vital in determining the photoactivity during the photodegradation process. Usually, the surface properties of TiO_2 intrinsically could be influenced by the preparation method, process, and doping, which determines the surface separation and transfer of charge carriers by generating surface states where electrons and holes are spatially trapped and transferred for subsequent redox reactions.

Compared to nonmetal dopant, substitution of metal ions can introduce an intraband state close to CB edge, which results in an obvious red shift in bandgap adsorption due to sub-band gap energies, such as transition metal doping [154–156], rare-earth metal doping [157–159], and other metal doping [160–162].

However, the diffusion of metal atoms is difficult in solid materials under low temperature. Consequently, it leads to inhomogeneous distributions of dopants and limited depth near a subsurface region. To obtain metal-doped TiO_2 nanoparticles with good homogeneity, sintering has to be conducted at a high temperature, which leads to particle agglomeration. Moreover, the metal dopants also provide more trapping sites for electrons and holes compared to nonmetal dopants. Furthermore, electron trapping occurs at a much faster process compared to hole trapping. In other words, trapping an electron or a hole is always ineffective for carrier separation because immobilized charge species rapidly recombine with its mobile counterparts. Last, metal doping has also some other drawbacks, especially thermal instability, which reduces the repeativity of TiO_2 photocatalysts. That is to say, it has a detrimental effect if the process is not under the control. Therefore, many researchers focused on the resolution of the above four problems in recent several years.

4.1. Transition metal element doping

Various properties of transition metal with 3*d* or 4*d* electron structure are influenced by many factors, such as the number of *d*-electrons on transition metal ions, crystalline structures, oxygen defects, and preparation methods [163–165]. Usually, the bandgap energy and band positions, Fermi level, and *d*-electron configuration of the electronic structure in TiO_2 can be effectively modulated when transition metal ions were introduced into TiO_2 lattice. Subsequently, it forms a wide range of new energy levels below CB arising from their partially filled *d*-orbitals, which results in an obvious red shift in bandgap and increases its visible light harvest [166, 167]. In addition, transition metal ions alter the carrier equilibrium concentration by serving as electron-hole trapping, suppress the recombination rate of electron-hole pairs, and enhance the degradation rates. That is, the photocatalytic performance for TiO_2 can be effectively improved through transition metal doping.

However, transition metal ions-doped TiO_2 appears to be a complex function of dopant concentration, energy level of dopant within the lattice, the *d* electron configuration, distribution of dopants, electron donor density, and incident light intensity. Every transition metal ion has different *d* electron configurations and its own characteristics. Therefore, it is important to further elaborate the process for every transition metal ion.

4.1.1. Iron (Fe) doping

Fe-doped TiO_2 shows superior activity due to its unique half-filled electronic configuration and shallow trapping compared to other metal dopants with closed shell electronic configuration, which can be more effective to influence the photoactivity [168–176]. Theoretical and experimental studies show that Fe doping can effectively reduce the trapping density and charge recombination, resulting in drastically improved adsorption.

Manu and Khadar synthesized Fe-doped TiO_2 nanocrystals at different atomic ratios through the hydrothermal method [168]. They found that the concentration of Fe dopants was more near the grain boundary because the dopant atoms were incorporated into the lattice at substitutional positions. The energy level associated with the peak at 2.63 eV was the deepest defect level. Consequently, the photocatalytic activity was enhanced greatly. Yan et al. developed a facile fast hydrolysis route to prepare a three-dimensional flow-like Fe-doped rutile TiO_2 nanostructure and investigated the relation between Fe doping and crystal planes [169]. Because the ionic radius of Fe was smaller than that of Ti, and the corresponding interplanar spacing distance of TiO_2 (110) was reduced with the replacement of Ti atoms by Fe atoms, as reflected by the shift of the (110) diffraction peak, which was similar with Liu and Zhang's result [170]. With Fe species doping into both the bulk phase and the surface, the bandgap narrowing of rutile TiO_2 was realized and the dissociative adsorption of water on the surface was promoted, which accordingly led to greatly enhanced activity in visible light-driven water oxidation.

4.1.2. Chromium (Cr) doping

Cr doping of TiO_2 also leads to a clear red shift in the UV-vis absorption spectrum, evidencing a decrease in bandgap and VB shift. Moreover, the Fermi level is also shifted to a higher energy by ~0 to 1 eV. With the change of preparation method and doped concentration, Cr-O anti-bond orbitals located slightly below the CBM in the region of ~3.0 to 2.2 eV and the unsaturated nonbonding *d* orbitals located in the middle of the gap region of ~2.5 to 1 eV. It also is suggested that Cr^{3+} doping is attributed to the increase of conductivity due to more free charges [177–180].

Li et al. synthesized Cr-doped TiO_2 via a hydrothermal method and found that Cr^{3+} ions could replace the Ti atoms in the lattice with oxygen vacancy compensation [177]. It was interesting that Cr doping also could prolong the lifetime of photogenerated carriers because the doped Cr^{3+} ions might act as the recombination centers of carriers.

4.1.3. Niobium (Nb) doping

Over the past few years, Nb-doped TiO_2 has received special attention due to its excellent electrical conductivity at room temperature. The ionic radius of Nb^{5+} of 0.064 nm is slightly larger than Ti^{4+} of 0.0605 nm. Therefore, Nb^{5+} works as an n-type dopant in TiO_2 lattice and generates additional carriers in its CB, which can notably increase photocatalytic performance [181–186].

Joshi et al. successfully prepared Nb-doped TiO_2 transparent films on glass substrates using a nonaqueous sol-gel spin coating technique [181]. Photocatalytic experiments showed that the films with 12 at.% Nb doping had excellent photocatalytic activity with 97.3% degradation of methylene blue after 2 h of UV irradiation. Archana et al. reported the high electron mobility and optical transparency of Nb-doped TiO_2, giving rise to the enhancement in charge transport behavior after 2 at.% Nb doping, which could assist the speedy initial reaction of the organic decomposition process and enhance the overall photocatalytic activity [182].

4.1.4. Other transition metal doping

Except above transition metal dopants, other transition metal atoms, including tungsten (W) [187–191], silver (Ag) [192–197], copper (Cu) [198, 199], cobalt (Co) [200–202], tantalum (Ta) [203–205], molybdenum (Mo) [206–208], zinc (Zn) [209–213], manganese (Mn) [214, 215], nickel (Ni) [216, 217], and vanadium (V) [218, 219], are also investigated by many researchers.

Recently, considerable enhancements of photocatalytic activity with W-doped TiO_2 in aqueous systems for the degradation of organic compounds have also been reported [187–191]. Liu et al. synthesized ordered mesoporous crystalline TiO_2 with various W doping level using SBA-15 as a hard template [187]. The existence of W ions expanded the range of useful excitation light to the visible spectra, greatly inhibited the recombination of electron-hole pairs on mesoporous TiO_2, and played an important role in improving the photocatalytic activity in the visible light region. The enhanced photocatalytic activity for W-doped TiO_2 could also be especially attributed to the presence of much higher Lewis surface acidity of a W-doped TiO_2 surface with a higher affinity for chemical species having unpaired electrons than pure TiO_2.

Ag is another important dopant in TiO_2 crystals and Ag doping can also cause an obvious shift towards narrowing the bandgap. Zhang et al. successfully synthesized Ag-doped TiO_2 with a novel hierarchical architecture via a combination of an electrospinning method and a hydrothermal process [192]. They found that Ag doping played a great role in the photocatalytic activity. Electron transfer to the Ag sites reduced the carrier recombination rate and allowed a more effective reaction between the surface trapped holes and electrons. However, excessive Ag dopant could also cause a decrease in the activity of TiO_2 because they occupied the active sites on the surface of the TiO_2. Moreover, the photogenerated electrons on the Ag sites attracted holes and recombined together.

Cu, as a kind of transition metal, is also found to be an effective dopant for TiO_2 to enhance the photocatalytic activity. Sajjad et al successfully prepared mesoporous Cu-doped TiO_2 via a sol-gel method at low temperature using water-immiscible room-temperature ionic liquid organic materials as a template and an effective additional solvent [198]. The results showed that Cu-doped TiO_2 samples exhibited superior visible light photocatalytic activities compared to undoped TiO_2 and P-25 [199, 200]. Further characterization indicated that Cu^+/Cu^{2+} sites as interfacial Ti-O-Cu surface linkages reduced bandgap energy as well as efficient charge separation due to the formation of Ti-O-Cu bonding at the surface and the associated appearance of oxygen vacancies, resulting in higher degradation rate.

Usually, Co dopant concentrations show weak influence on photocatalytic performance, whereas the oxygen vacancy concentration and distribution in the system show much stronger influence on the optical performance due to the shift of Fermi level up by ~0.75 eV [201]. Cai et al. presented a controllable and reliable method to synthesize Co-doped TiO_2 nanowires through a combining versatile solution phase chemistry and rapid flame annealing process [202]. They found an enhanced catalytic activity in Co-doped TiO_2 crystals. However, Co doping was also shown to drastically deteriorate performance at high doping concentration due to the formation of sub-band gap states that act as recombination centers.

Sengele et al. obtained Ta-doped TiO_2 via a sol-gel route and found that the Ta doping could induce significant modifications on the structural, morphological, surface, electronic, and optical properties of TiO_2 [203]. Total diethylsulfide elimination could be reached for 100 min under continuous contaminant flux before deactivation and the conversion maintained to 80% of degradation after 200 min, which was higher than undoped TiO_2 catalysts [204–208].

Recently, many researchers found that transition metal could effectively modulate the crystal face, which could improve photocatalytic performance [209–213]. Saad et al. synthesized Zn-doped TiO_2 nanowall with a (001) facet and porous structure [209]. They found that the samples with a (001) facet exhibited enhanced photocatalytic activity and Zn-doped TiO_2 had better degradation rates compared to other samples.

4.2. Rare-earth metal doping

Another path to achieve the abovementioned goal is represented by rare-earth doping [214–219]. Compared to transition metals, rare-earth metals with 4*f*, 5*d*, and $6s^2$ states are considered as the ideal dopants to modify the crystal structure, electronic structure, and optical properties

of TiO_2, which can effectively influence the positions, widths, and density of states of CB and VB [220, 221]. Furthermore, rare-earth metals can form complexes with various Lewis-based organic compounds through interaction of the functional groups with their *f* orbital, thereby improving the photoactivity. Last, the functional integration of upconversion luminescent rare-earth ions with photocatalyst provides a potential for wavelength conversion and efficient utilization of solar energy for this purpose [222, 223]. This approach appears to be a completely new alternative for enhancing the efficiency of the photocatalytic process. In other words, the applications of the upconversion process by phosphor-like systems can optimize the photocatalytic performance of traditional UV active photocatalysts.

Therein, lanthanide (La) has been widely used and investigated in the field of optical application (LED light, laser, photocatalytic, solar cell, etc.). Particularly, the ability of these nanomaterials to release high-energy photons after NIR laser-light stimulation allows deep tissue imaging and luminescent nanoparticles [224, 225]. Du et al. prepared pure and La-doped TiO_2 thin films via a sol-gel method using tetrabutyl titanate as Ti precursors [224]. The results showed that the content of La was the key factor for hydrophilic and photocatalytic activity. $LaTiO_3$ could be formed in La-doped TiO_2 thin films, which caused the TiO_2 lattice distortion and restrained the transition from anatase to rutile. By adding 0.3 wt.% La to the TiO_2 thin films, 92.02% methylene blue was finally degraded.

Cerium (Ce), as a typical rare-earth metal, is widely used to dope TiO_2 because of its unique electronic structure. The main feature of Ce ion doping is the different electronic structures of 4*f* states, such as Ce^{3+} with $4f^15d^0$ and Ce^{4+} with $4f^05d^0$. The visible light photoactivity of Ce-doped TiO_2 nanoparticles is mainly due to the presence of 4*f* level in the mid-bandgap of TiO_2 crystals, which leads to the optical absorption between 400 and 500 nm. The possible transition of *d* and *f* orbital electrons can also reduce the recombination rate of electron-hole pairs, thereby making TiO_2 more feasible for photocatalytic response under visible light [226–229]. Maddila et al. prepared Ce-doped TiO_2 catalysts using a wet impregnation method [226]. The results indicated that Ce-doped TiO_2 exhibited an obvious red shift, reducing the bandgap and improving the photocatalytic efficiency. Photocatalyzed ozonation with 1at.% Ce/TiO_2 yielded 100% degradation in 2 h under basic pH conditions.

Among various upconverting nanomaterials, erbium (Er) can be excited by NIR or visible light [230–232]. Obregon and Colon synthesized Er-doped TiO_2 through a surfactant free hydrothermal method, which exhibited good photoactivities under sun-like excitation for the degradation of phenol [231]. The presence of Er^{3+} did not affect the structural and morphological features of the TiO_2 significantly, whereas photocatalytic experiments clearly evidenced that Er introduction into TiO_2 matrix would promote the profiting of NIR photons, enhancing the photoactivity of the catalyst.

Gadolinium (Gd) doping raises VB maximum with respect to the Fermi level and thus turns the intrinsic virgin phase into a p-type semiconductor. Choi et al. synthesized three-dimensional Gd-doped TiO_2 nanofibers using a simple electrospinning technique [233]. The pristine Gd-doped TiO_2 nanofibers showed a higher photocatalytic activity than the TiO_2 nanoparticles, which could be attributed to the fast electron transport. In addition, Gd-doped TiO_2 nanofibers

showed nearly five-fold enhancement in the photocatalytic degradation rate due to synergistically higher electron transport.

Europium (Eu) is also a good candidate for upconversion materials and is widely used in the field of photocatalyst, laser, solar cell, etc. Recently, many researchers also attempted to dope Eu into TiO_2 lattice [234–236]. Leroy et al. prepared periodic mesoporous Eu-doped TiO_2 through the EISA process [234]. They found that strong fluctuations existed in the intensity of the $^5D_0 \rightarrow {}^7F_2$ transition under UV light exposure. Correlation of the emission with the photocatalytic activity of the semiconductor for the photodegradation of an organic molecule could also be firmed.

Yttrium (Y) doping usually shows weak influence on bandgap energy and does not alter the Fermi level. However, it can increase hole mobility to generate p-type TiO_2, which is helpful for the carrier transport. Wu et al. prepared a novel mesoporous Y-doped TiO_2 nanosheet array via a low-cost, facile, and template-free solvothermal method by employing waste tricolor fluorescent powder (WTFP) as a dopant Y source and acetic acid as a mesopore template [237]. The 2.5 and 5 wt.% Y-doped TiO_2 films showed higher photocatalytic activity for the methyl orange, with 82.6% and 81.3% reduction within 6 h irradiation, respectively. The enhanced photocatalytic activity of Y-doped TiO_2 film was attributed to the large surface area and the low electron-hole recombination rate as well as enhanced absorption of organic pollutants on the semiconductor surface. Li et al. also confirmed that ytterbium (Yb) doping was also a kind of route to improve the NIR photocatalytic degradation of rhodamine B [238].

4.3. Other metal dopants

Recently, many researchers found that lithium (Li) doping plays an important role in the inhibition of activity in the TiO_2 network acting as an electron trapping or hole trapping [239–241]. Bouattour et al. reported Li-doped TiO_2 nanoparticles through a sol-gel process and investigated their potential application as a photocatalyst for degradation of different organic compounds [240]. Results showed that an inhibition of activity is presented in the Li doping network. However, the surface accumulation of Li^+ on TiO_2 particles could favor better interfacial charge transfer.

Long et al. calculated the electronic structures of silicon (Si)-, germanium (Ge)-, tin (Sn)-, and lead (Pb)-doped anatase and rutile TiO_2 systematically using DFT calculations [242]. Doping with Si, Ge, Sn, and Pb elements also narrowed the bandgap of rutile TiO_2 due to a shift far away from the CB minimum. The reduction of the bandgap is 0.20 and 0.15 eV in Si- and Ge-doped anatase TiO_2, respectively. However, there were enlargements of 0.06 and 0.02 eV in the bandgap of Sn- and Pb-doped anatase TiO_2, respectively. They predicted that Ge-doped TiO_2 was efficient for the overall water splitting using visible light irradiation.

Doping with bismuth (Bi) ions can also decrease the bandgap of TiO_2 and thereby extend its absorption into the visible light region, enhancing its photocatalytic efficiency [243–245]. The impurity energy level from the hybrid of Bi 6s, O 2*p*, and Ti 3*d* orbitals is the cause of the red shift of the absorption edge. Therefore, Bi-doped TiO_2 systems are more effective for the photodegradation of organic pollutants under visible light irradiation, such as methyl blue

and methyl orange. Wu et al. developed a facile method to prepare Bi-doped TiO_2 through hydrothermal synthesis followed by thermal annealing treatment [243]. Bi doping caused the formation of Bi_xTiO_y and reduced bandgap widths. Moreover, some special structural defects created by the migration of Bi^{3+} ions were also responsible for the high photoactivity. Bi-doped TiO_2 catalysts with high doping concentration (such as 5 and 10 mol%) showed the highest activity for the catalyzed photodegradation of methyl orange under visible light irradiation.

Sn doping is another important supplementary form to improve photocatalytic performance [246, 247]. Oropeza et al. investigated the influence of Sn doping on the anatase to rutile phase transition, as well as the photocatalytic performance [246]. They found that Sn-doped TiO_2 exhibited enhanced visible light region photocatalytic activity compared to undoped TiO_2 in dye degradation experiments, even it was higher than that of N-doped TiO_2. This was attributed to the narrowing of the bulk bandgap at low doping levels. The Sn surface states laid above the VB top and could therefore act as trapping sites for holes.

5. Codoping

Although the monodoped nonmetal or metal atoms can obviously enhance photocatalytic performance, they always act as the recombination centers because of the partially occupied impurity bands. It has been recognized theoretically that codoping using two or more foreign atoms can passivate the impurity bands and decrease the formation of recombination centers by increasing the solubility limit of dopants. Furthermore, codoping can also modulate the charge equilibrium. Consequently, codoping can effectively enhance the photocatalytic activity. Based on the research of doping effects, two or more elements are introduced into TiO_2 lattice to check the changes of electronic structure and bandgap energy, including nonmetal and nonmetal atoms [248–250], nonmetal and metal atoms [251–253], and metal and metal atoms [254–256].

Regardless of whether doping is based on single heteroatoms or coupled heteroatoms, the spectral distribution and localized states in the bandgap essentially determine the visible light absorbance and redox potential of the photo-induced charge carriers. Therefore, it is a challenge and hot topic to introduce different dopants, which can realize substantial synergistic effects.

5.1. Nonmetal-nonmetal doping

5.1.1. N-nonmetal codoping

To improve the photocatalytic performance of N-doped TiO_2 catalysts, the modification strategy has been extensively adopted and investigated by many researchers, such as N-nonmetal codoping, C-nonmetal codoping, and other nonmetal-nonmetal codoping. The modified N-doped TiO_2 usually showed favorable effects for improving the photocatalytic activity in the range of visible light compared to N-doped TiO_2.

Therein, the (N, S) codoping TiO_2 can play a vital role in significantly improving photocatalytic activity because of the strong synergistic interaction between S and N, in which the surface separation of photoexcited electron-hole pairs is promoted [257–259]. Consequently, the VB of TiO_2 shifts to a positive direction, which leads to higher oxidative ability and degradation ability towards pollutant under visible light irradiation. Etacheri et al. further proved that the formation of isolated S 3p, N 2*p*, and π^* N-O states between the VB and CB was responsible for the visible light absorption [260].

Chung et al. synthesized the (N, S) codoped TiO_2 with an anatase phase using a simple solvothermal treatment and investigated their visible light photocatalytic activity associated with the thermal behavior [257]. They found that the (N, S) codoped TiO_2 had better visible light photocatalytic activity and adsorptivity than the commercially available P25. The S dopants effectively assisted the surface reaction by adsorbing cations of organic dyes on the codoped TiO_2 surface. The N dopants formed a delocalized state in the bandgap, which led to the enhanced solution bulk reaction by increasing visible light absorbance (**Figure 4**).

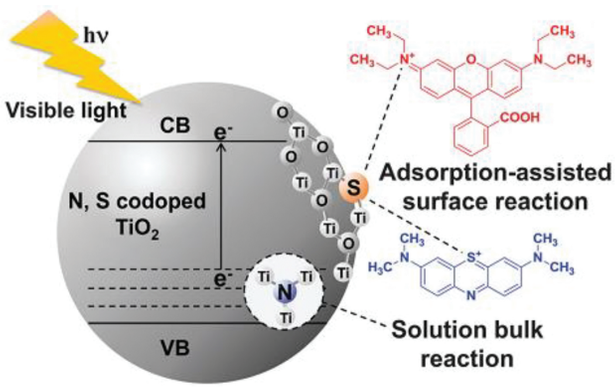

Figure 4. Schematic illustration of the suggested effects of N and S dopants on the enhanced visible light photocatalytic activity of TiO_2 [257].

It is noteworthy that (N, S) codoping can also effectively modulate the preferential growth plane of TiO_2 crystals. Xiang et al. prepared (N, S) codoped TiO_2 nanosheets with exposed {001} facets by a simple mixing-calcination method using the hydrothermally prepared TiO_2 nanosheets as a precursor and thiourea as a dopants [261]. The first-principles DFT proved that the electrons could be easily excited in the impurity states and then migrated between VB and intermediate. These resulted in stronger absorption with a red shift in the bandgap transition.

Recently, Samsudin et al. used (N, F) codoping to improve the intrinsic properties of the TiO_2 catalyst and found that the (N, F) codoping not only introduced activity in the visible light region but also improved the performances of intrinsic TiO_2 itself. The high activity could be attributed to the presence of N and F, which resulted in the change in the morphology and increasing presence of {001} facets [262]. Subsequently, a great number of experiments and theoretical calculations were carried out to further discuss (N, F) codoping in TiO_2 crystals [263–267]. Rahul and Sandhyarani synthesized three-dimensionally ordered (N, F) codoped

TiO_2 by templating with polystyrene colloidal photonic crystals using nitric acid and trifluoroacetic acid as raw materials and found an obvious red shift due to (N, F) codoping [263]. Further investigation showed that the enhancement of photocatalytic activity could be attributed to the bandgap scattering effect and the slow photon effect, leading to a significant improvement in solar light harvesting.

(N, B) codoped TiO_2 is also an effective approach to improve photocatalytic activity [268–270]. Usually, N and B atoms are interstitial species connected to the same O lattice. The energy level of the [NOB] species is located close to edge of the VB and lies below the corresponding level of $[N_iO]$• because of the electrostatic stabilization. In other words, the photocatalytic activities are influenced not by [NOB] center but by [NOB]• center located at higher energy level. Moreover, the presence of N and B species can effectively narrow the bandgap and inhibit the transformation of anatase TiO_2 to rutile phase [269].

Other N-nonmetal codoping includes (N, C) codoping [271, 272] and (N, H) codoping [273, 274]. Liu et al. exploited (N, C) codoped porous TiO_2 nanofibers by a combination of electrospinning and controlled calcination technologies [271]. The codoping of N and C in TiO_2 not only led to a shift of the absorption edge to lower energy by inducing new band levels but also created a large amount of single electron-trapped oxygen vacancies. Recently, Wei et al. demonstrated a new chemical approach to prepare black anatase TiO_{2-x} and yellow anatase TiO_2 nanoparticles by doping with N and H [273]. The substitutional nonmetal doping of N and H, especially the *p* states of N, contributed to the bandgap narrowing by mixing with O 2*p* states and formed the new VB. Theoretical work suggested that the adequately high concentration of Ti^{3+} could induce a continuous oxygen vacancy of electronic states just below the CB edge of TiO_2, which strongly enhanced visible light absorption and the photocatalytic performance of the catalysts under visible light. The bandgap energy of the samples also decreased substantially, which was narrowed to about 2.0 eV.

5.1.2. C-nonmetal codoping

C-nonmetal codoping is also a kind of common approach to improve photocatalytic activity, such as (C, B) codoping [275, 276], (C, F) codoping [277], and (C, S) codoping [278].

Yu et al. investigated the geometry structures, formation energies, and electronic properties of the C, B and (C, B)-doped anatase TiO_2 using DFT calculations [275]. The results implied that (C, B)-codoped anatase TiO_2 could markedly influence the photocatalytic activity and light adsorption due to the change of the energy gaps (E_g) and Fermi levels (E_F). Moreover, the separation efficiency of carriers could be improved because of the existence of Ti^{3+} ions. Lin et al. systematically investigated the electronic and optical properties of several possible (C, B) codoped models of anatase and rutile TiO_2 using DFT calculations [276]. The further calculation indicated that B 2*p* and C 2*p* decreased the bandgap by about 0.8 eV and the couples of the two hybridized states could also result in a downward red shift for spectrum response.

Deng et al. prepared F-modified C-doped TiO_2 composites via a simple sol-gel method using NaF as the F source followed by heat treatment at 700°C in N atmosphere [277]. The C atoms and F species interacted in the TiO_2 lattice and resulted in the narrowed bandgap (2.50 eV),

which could inhibited the recombination of photo-induced irradiation and resulted in a superior photocatalytic activity.

5.1.3. Other nonmetal-nonmetal codoping

Except for the above N-nonmetal codoping and C-nonmetal codoping, other nonmetal atoms, including (B, P) codoping [279], (B, F) codoping [280], and tridoping [281–284], are also investigated by many researchers. Yu et al. prepared a series of TiO_2 hollow sphere catalysts with or without nonmetal (B, P) dopants through a sol-gel process with styrene-methyl methacrylate copolymer microspheres as the template [279]. They found that both B and P dopants could also narrow the bandgap of the TiO_2 catalyst.

Recently, many researchers found that tridoping in TiO_2 crystals is an effectively supplemental tool. Ramanathan and Bansal synthesized (N, C, F) tridoped rutile TiO_2 nanorods that not only displayed enhanced photocatalytic performance in UV light but also allowed a significant level of visible light photocatalytic activity [281]. In visible light, pure TiO_2 only got 6% photodegradation of Congo red over 30 min, whereas (N, C, F) tridoped TiO_2 caused 56% dye degradation.

5.2. Metal-metal codoping

Although monometal doping can improve the bandgap structure, the serious recombination centers also deteriorate carrier transport due to its partially occupied impurity bands. Hence, many researchers want to improve carrier transport through codoping with two different metal elements, such as (Ti, Ni) codoping [285], (Ti, Fe) codoping [286], (Ag, W) codoping [287], (Ag, Zr) codoping [288], (Zn, Mn) codoping [289], (Cu, V) codoping [290], and (Fe, Ce) codoping [291].

Zhang et al. developed a novel Ni^{2+} and Ti^{3+} codoped porous anatase TiO_2 via a facile sol-gel technique combined with an *in situ* solid-state chemical reduction approach followed by mild calcinations (350°C) in Ar atmosphere [285]. The results showed that the doping of Ti^{3+} and Ni^{2+} species for TiO_2 could result in the tail states and significantly narrowed the bandgap of

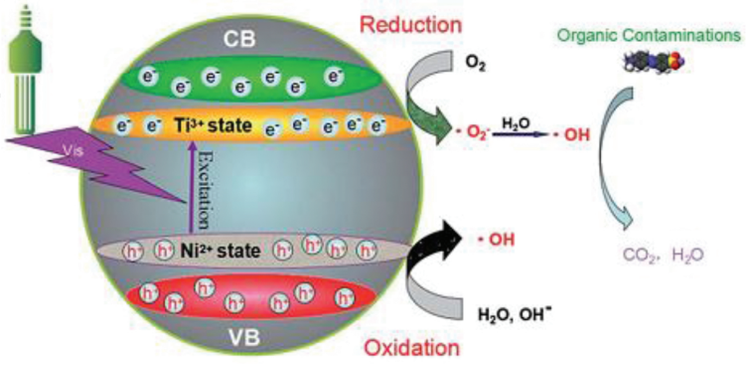

Figure 5. Schematic diagram of the photocatalytic process for Ni^{2+} and Ti^{3+} codoped TiO_2 under visible light irradiation [285].

anatase TiO_2 due to the formation of midgap states. Namely, Ti^{3+} state below CB minimum and Ni^{2+} state above VB maximum would be helpful in light adsorption and slowed the carrier recombination (**Figure 5**). In other words, (Ti, Ni) codoped porous black anatase TiO_2 resulted higher photocatalytic performance for methyl orange and rhodamine B.

Chen et al. found that Fe^{3+}/Ti^{3+} codoping was also a good way to further improve Ti^{3+} self-doping TiO_2 photocatalyst [286]. Fe^{3+} doping could result in a blue shift for the VB edge by 1.0 eV. The synergistic effects between Ti^{3+} and Fe^{3+} dopants in the samples significantly narrowed the bandgap, leading to efficient photocatalytic performance in the visible light range.

Khan et al. synthesized (Ag, W) codoped TiO_2 with different W doping concentrations using the hydrothermal method [287]. The codoped TiO_2 displayed pure anatase phase with strong absorption in visible light region. Among all the codoped samples, the one with W doping concentration of 3.5 at.% possessed the best photocatalytic activity, which was attributed to the synergistic effect between the dopants and optimal doping concentration.

Benjwal and Kar investigated (Zn, Mn) codoped TiO_2 photocatalysts through varying dopant concentrations and found that the highest photocatalytic degradation of methyl blue was obtained with 1.0 at.% (Zn, Mn) codoped TiO_2 [289]. Further analysis showed that the incorporation of Zn^{2+} and Mn^{2+} ions into TiO_2 lattice caused a decrease of the energy bandgap due to the formation of impurity levels below VB, which resulted in an enhancement of light absorbance in the UV region. With further increasing codoping concentration, the density of new energy levels also increased, which ultimately enhanced the recombination possibilities of electron and holes because they could be easily trapped on these recombination centers.

Christoforidis and Fernández-García prepared two series of Cu^{2+} and V^{4+} codoped anatase TiO_2 samples using the microemulsion synthetic route by varying the metal/Ti ratio [290]. They found that isolated and highly dispersed Cu^{2+} and V^{4+} species favored the hole formation while at the same time decreased the amount of Ti^{3+} centers under irradiation. Therefore, it could be deduced that (Cu, V) codoping contributed to the better photocatalytic performance due to the faster carrier separation.

Visible light-sensitive Fe^{3+} and Ce^{4+} codoped nano-TiO_2 photocatalyst was also investigated by Jaimy et al. [291]. They concluded that Fe doping and Ce doping could improve the light adsorption through trapping carriers and bending the VB and CB, respectively. In other words, the recombination of photoexcited electrons and holes was obviously prevented. Consequently, the codoped TiO_2 compositions exhibited higher photocatalytic activity than that of pure TiO_2 and commercial Degussa P25 under visible light.

5.3. Nonmetal-metal doping

5.3.1. N-metal doping

Recently, many researches about metal and N comodified TiO_2 indicate that metal assist N doping into the lattice TiO_2 and enhanced the shift of absorption edge to the visible light range, such as La, Ti, Zn, W, Cu, Fe, Ni, V, Cr, Ce, and Mn. Usually, N doping can form new states lying just above the VB, whereas the metal ion incorporated into the lattice TiO_2 or dispersed

on the surface of TiO_2 can enhance the separation rate of photogenerated charges. Under visible light irradiation, the electron can be excited from the N impurity level to the metal ion impurity level or from the N impurity level to the CB or from the VB to the metal ion impurity level. This strategy has been extensively adopted to design visible-active photocatalysts with high efficiency.

Sun et al. [292] and Yu et al. [293] investigated the interaction between substitutional N and implanted La at the (101) and {001} facets of TiO_2 using first-principles DFT calculations and analyzed the origin of enhanced visible light photocatalytic activity of (N, La) codoped TiO_2. They found that substitutional probability of N atom obviously decreased due to La implantation. However, oxygen vacancies were greatly enhanced because of the synergistic effects of La doping and N doping. For the substitutional La/N codoped surface, the charge compensation between the substitutional La and substitutional N led to the formation of two isolated occupied N(s)-O π^* impurity levels in the gap, forming the acceptor-donor-acceptor compensation pair and providing a reasonable mechanism for the enhanced visible light photocatalytic activity of (N, La) codoped TiO_2 anatase.

Li et al. developed a facile solvothermal strategy to simultaneously realize N doping and Ti^{3+} self-doping in TiO_2 crystals [294]. N doping and concomitant Ti^{3+} incorporation accounted for the reduction of the bandgap and realized photocatalytic activity in the visible light region. In other words, the introduced Ti^{3+} ions could form a new sublevel state below the CB and thus generate more electrons and holes, which combined with the midgap state induced by N doping, synergistically reduced the bandgap to a lower level and finally improved the response to visible light. Consequently, (N, Ti) codoped hierarchical anatase TiO_2 catalysts manifested an excellent photocatalytic activity, deriving from its superior light harvesting ability, narrowing bandgap from the codoping strategy, enhancing adsorption capacity, and accelerating carrier transport rate.

A new type of (N, Zn) codoped TiO_2 photocatalyst was prepared by Wang et al. via a simple sol-gel technique, which exhibited a higher photocatalytic activity than pure TiO_2, N-doped TiO_2, and Sn-doped TiO_2 under both visible and UV light irradiation [295]. This implied that (N, Zn) codoping was a more efficient way to improve the photocatalytic activity than doping with just one type of ion. Hu et al. further confirmed the above results through nitridation and hydrogenation of a zinc titanium precursor [296].

(N, W) codoping is also an efficient way to improve the recombination of photogenerated carriers [297, 298]. Lai and Wu prepared (N, W) codoped TiO_2 nanobelt through a facile and low-temperature route followed by a subsequent calcination [297]. The achieved nanobelt film possessed a reduced bandgap of approximately 2.3 eV at approximately 2.6 at.% W and 3.1 at. % N. Moreover, the single N-doped, W-doped, and (N, W) codoped TiO_2 induced photodegradations of 88%, 73%, and 95% rhodamine B molecules, respectively. The higher activity of the (N, W) codoped TiO_2 further supported the positively synergetic effects arising from the codoping.

Recently, some researchers develop a novel (N, Cu) codoped TiO_2 photocatalysts and also find that the photocatalytic effect was good. For example, Wang et al. found that 7.7% of methyl

blue were adsorbed on the surface of (N, Cu) codoped TiO_2 nanosheet when the adsorption reached equilibrium in the dark, whereas 5.9% of methyl blue were adsorbed on the control sample [299]. The relatively low adsorption of methyl blue might be attributed to the low surface area of the N-doped TiO_2 nanosheet, and the slightly enhanced adsorption for (N, Cu) codoped TiO_2 nanosheet might be attributed to its modified surface by the Cu doping.

Zhang et al. prepared TiO_2 nanotubes codoped with Fe and N using a one-step hydrothermal method [300]. Compared to the commercial TiO_2 powders and pure TiO_2 nanotubes, (N, Fe) codoped TiO_2 nanotubes exhibited a stronger visible light absorption capability and an enhanced photocatalytic activity under visible light irradiation. The increase in photocatalytic activity could be ascribed to the narrowing of the bandgap and the promoted separation of the photogenerated electrons and holes. Fe^{3+} ions were thought to occupy the active sites on the surface of (N, Fe) codoped TiO_2 as recombination centers for the electrons and holes.

Other N and metal codoping also includes (N, Ni) codoping [301], (N, Bi) codoping [302], (N, V) codoping [303], and (N, Mo) codoping [304]. Liu et al. reported the facile synthesis of reduced (N, Ni) codoped TiO_2 nanotubes and their photocatalytic activity application [301]. The narrowed bandgap of TiO_2 due to the doping of N and Ni elements could enhance the light absorption effectively. The electrochemical characterization revealed that photo-induced carriers were more efficient charge separation and transportation in reduced (N, Ni) codoped TiO_2 nanotubes photoanodes.

5.3.2. S-metal codoping

Recently, S-metal codoping has also been widely researched, such as (S, Fe) codoping [305], (S, Mo) codoping [306], and (S, Cu) codoping [307]. He et al. found that S and Fe could be easily implanted into the lattice of TiO_2 via a precipitation method [305]. Compared to undoped TiO_2, (S, Fe) codoped TiO_2 showed a higher photocatalytic activity under both UV and visible light irradiation, and the optimal methyl blue degradation level was 96.92%.

Zhang also developed for the first time a one-step hydrothermal process to synthesize (S, Mo) codoped TiO_2 mesoporous nanospheres [306]. The photodegradation ability towards rhodamine B was 3.8 times higher than that of the only S-doped samples.

5.3.3. Other nonmetal-metal doping

(F, Ca) codoped TiO_2 also caused several beneficial effects, including the enhancement of surface acidity, creation of oxygen vacancies, and increase of active sites as well as an impurity energy state (2.0 eV) below the CB of TiO_2, which could shorten the excitation path of electrons and reduce the apparent bandgap [308]. The smaller crystal size caused by doping with Ca could exhibit more powerful redox ability and the efficient separation of photogenerated electron-hole pairs. This implied that (F, Ca) codoping might be a kind of efficient way to improve the photocatalytic activity of TiO_2.

(B,Co) codoped TiO_2 was also investigated by Jaiswal et al. via DFT calculations [309]. They found that B occupied the interstitial site at low concentration (1 at.%), whereas it occupied

substitutional O position as the concentration increased (2 and 3 at.%). Both these B-doped TiO_2 showed improved photocatalytic activity due to the formation of shallow energy level, whereas higher visible light absorption was achieved owing to the presence of two deep energy levels in the bandgap according to DFT calculations.

Recently, a series of tridoped has also been developed [310, 311]. For example, Li et al. prepared (Cu, Ce, B) tridoped TiO_2 nanotubes via a hydrothermal method assisted by cetyl trimethyl ammonium bromide [310]. They found that Cu, Ce, and B could be intercalated into the interlayer spacing of the nanotubes besides the substitution for the Ti^{4+} or O_2^-. The synergetic effect of narrowing the bandgap of (Cu, Ce, B) tridoping exhibited the highest photocatalytic activity, which greatly inhibited the recombination of electrons and holes and enhanced the concentration of photogenerated carriers.

Acknowledgements

The work was financially supported by Jiangsu Province Natural Science Foundation (BK20141133 and BK20130195), Fundamental Research Funds for the Central Universities (2015XKMS096), China Postdoctoral Science Foundation (2015M580488), and Scientific Research Foundation of Key Laboratory of Coal-Based CO_2 Capture and Geological Storage of Jiangsu Province (China University of Mining and Technology, 2015B05).

Author details

Fei Huang[1,2*], Aihua Yan[1,2] and Hui Zhao[2]

*Address all correspondence to: huangfei7804@163.com

1 Low Carbon Energy Institute, China University of Mining and Technology, Xuzhou, China

2 School of Materials Science and Engineering, China University of Mining and Technology, Xuzhou, China

References

[1] F. Spadavecchia, M. Ceotto, L. L. Presti, C. Aieta, I. Biraghi, D. Meroni, S. Ardizzone, G. Cappelletti. Second generation nitrogen doped titania nanoparticles: A comprehensive electronic and microstructural picture. Chin. J. Chem., 2014, 32, 1195–1213.

[2] N. Yamada, M. Suzumura, F. Koiwa, N. Negishi. Differences in elimination efficiencies of *Escherichia coli* in freshwater and seawater as a result of TiO_2 photocatalysis. Water Res., 2013, 47, 2770–2776.

[3] F. D. Angelis, C. D. Valentin, S. Fantacci, A. Vittadini, A. Selloni. Theoretical studies on anatase and less common TiO_2 phases: Bulk, surfaces, and nanomaterials. Chem. Rev., 2014, 114(19), 9708–9753.

[4] Z. Zheng, J. Zhao, Y. Yuan, H. Liu, D. Yang, S. Sarina, H. Zhang, E. R. Waclawika, H. Zhu. Tuning the surface structure of nitrogen-doped TiO_2 nanofibres—An effective method to enhance photocatalytic activities of visible-light-driven green synthesis and degradation. Chem. Eur. J., 2013, 19, 5731–5741.

[5] B. Zheng, Q. Guo, D. Wang, H. Zhang, Y. Zhu, S. Zhou. Energy-transfer modulation for enhanced photocatalytic activity of near-infrared upconversion photocatalyst. J. Am. Ceram. Soc., 2015, 98(1), 136–140.

[6] L. Liu, X. B. Chen. Titanium dioxide nanomaterials: Self-structural modifications. Chem. Rev., 2014, 114, 9890–9918.

[7] F. Zuo, K. Bozhilov, R. J. Dillon, L. Wang, P. Smith, X. Zhao, C. Bardeen, P. Y. Feng. Active facets on titanium (III)-doped TiO_2: An effective strategy to improve the visible-light photocatalytic activity. Angew. Chem. Int. Ed., 2012, 124, 6327–6330.

[8] M. Xing, X. Li, J. Zhang. Synergistic effect on the visible light activity of Ti^{3+} doped TiO_2 nanorods/boron doped graphene composite. Sci. Rep., 2014, 4, 5493–5499.

[9] S. X. Liu, J. L. Liu, X. S. Li, X. Zhu, A. M. Zhu. Gliding arc plasma synthesis of visible-light active C-doped titania photocatalysts. Plasma Process. Polym., 2015, 12, 422–430.

[10] R. Marschall, L. Wang. Non-metal doping of transition metal oxides for visible-light photocatalysis. Catal. Today, 2014, 225(15), 111–135.

[11] M. Li, S. Zhang, Y. Peng, L. Lv, B. Pan. Enhanced visible light responsive photocatalytic activity of TiO_2-based nanocrystallites: Impact of doping sequence. RSC Adv., 2015, 5, 7363–7369.

[12] K. Song, X. Han, G. Shao. Electronic properties of rutile TiO_2 doped with 4*d* transition metals: First-principles study. J. Alloy Compd., 2013, 551, 118–124.

[13] X. Yu, T. Hou, X. Sun, Y. Li. The influence of defects on Mo-doped TiO_2 by first-principles studies. Chem. Phys. Chem., 2012, 13, 1514–1521.

[14] F. D. Angelis, S. Fantacci, A. Selloni, M. Grätzel, M. K. Nazeeruddin. Influence of the sensitizer adsorption mode on the open-circuit potential of dye-sensitized solar cells. Nano Lett., 2007, 7, 3189–3195.

[15] M. Borlaf, M. T. Colomer, A. de Andrés, F. Cabello, R. Serna, R. Moreno. TiO_2/Eu^{3+} thin films with high photoluminescence emission prepared by electrophoretic deposition from nanoparticulate sols. Eur. J. Inorg. Chem., 2014, 5152–5159.

[16] N. Umezawa, J. Ye. Role of complex defects in photocatalytic activities of nitrogen-doped anatase TiO_2. Phys. Chem. Chem. Phys., 2012, 14, 5924–5934.

[17] H. Lin, L. Li, M. Zhao, X. Huang, X. Chen, G. Li, R. Yu. Synthesis of high-quality brookite TiO_2 single-crystalline nanosheets with specific facets exposed: Tuning catalysts from inert to highly reactive. J. Am. Chem. Soc., 2012, 134, 8328–8331.

[18] M. Zhao, H. Xu, H. Chen, S. Ouyang, N. Umezawa, D. Wang, J. Ye. Photocatalytic reactivity of {121} and {211} facets of brookite TiO_2 crystals. J. Mater. Chem. A, 2015, 3, 2331–2337.

[19] C. C. Mao, H. S. Weng. Effect of heat treatment on photocatalytic activity of titania incorporated with carbon black for degradation of methyl orange. Environ. Prog. Sustain. Energ., 2012, 31(2), 306–317.

[20] M. L. Satuf, R. J. Brandi, A. E. Cassano, O. M. Alfano. Photocatalytic degradation of 4-chlorophenol: A kinetic study. Appl. Catal. B Environ., 2008, 82(1), 37–49.

[21] X. Jiang, Y. Zhang, J. Jiang, Y. Rong, Y. Wang, Y. Wu, C. Pan. Characterization of oxygen vacancy associates within hydrogenated TiO_2: A positron annihilation study. J. Phys. Chem. C, 2012, 116, 22619–22624.

[22] A. Eslami, M. M. Amini, A. R. Yazdanbakhshc, A. Mohseni-Bandpei, A. A. Safari, A. Asadi. N, S co-doped TiO_2 nanoparticles and nanosheets in simulated solar light for photocatalytic degradation of non-steroidal anti-inflammatory drugs in water: A comparative study. J. Chem. Technol. Biot., 2016, doi: 10.1002/jctb.4877.

[23] I. N. Martyanov, S. Uma, S. Rodrigues, K. J. Klabunde. Structural defects cause TiO_2-based photocatalysts to be active in visible light. Chem. Commun., 2004, 21, 2476–2477.

[24] A. Naldoni, M. Allieta, S. Santangelo, M. Marelli, F. Fabbri, S. Cappelli, C. L. Bianchi, R. Psaro, V. D. Santo. Effect of nature and location of defects on bandgap narrowing in black TiO_2 nanoparticles. J. Am. Chem. Soc., 2012, 134, 7600–7603.

[25] J. Cai, Z. Huang, K. Lv, J. Sun, K. Deng. Ti powder-assisted synthesis of Ti^{3+} self-doped TiO_2 nanosheets with enhanced visible-light photoactivity. RSC Adv., 2014, 4, 19588–19593.

[26] G. Li, Z. Lian, X. Li, Y. Xu, W. Wang, D. Zhang, F. Tian, H. Li. Ionothermal synthesis of black Ti^{3+}-doped single-crystal TiO_2 as an active photocatalyst for pollutant degradation and H_2 generation. J. Mater. Chem. A, 2015, 3, 3748–3756.

[27] J. Huo, Y. Hu, H. Jiang, C. Li. *In situ* surface hydrogenation synthesis of Ti^{3+} self-doped TiO_2 with enhanced visible light photoactivity. Nanoscale, 2014, 6, 9078–9084.

[28] Z. Zheng, B. Huang, X. Meng, J. Wang, S. Wang, Z. Lou, Z. Wang, X. Qin, X. Zhang, Y. Dai. Metallic zinc-assisted synthesis of Ti^{3+} self-doped TiO_2 with tunable phase composition and visible-light photocatalytic activity. Chem. Commun., 2013, 49, 868–870.

[29] I. Justicia, P. Ordejon, G. Canto, J. L. Mozos, J. Fraxedas, G. A. Battiston, R. Gerbasi, A. Figueras. Designed self-doped titanium oxide thin films for efficient visible-light potocatalysis. Adv. Mater., 2002, 14, 1399–1402.

[30] F. Zuo, L. Wang, T. Wu, Z. Zhang, D. Borchardt, P. Feng. Self-doped Ti^{3+} enhanced photocatalytic for hydrogen production under visible light. J. Am. Chem. Soc., 2010, 132(34), 11856–11857.

[31] G. Lu, A. Linsebigler, J. T. Yates. Ti^{3+} defect sites on TiO_2(110): Production and chemical detection of active sites. J. Phys. Chem., 1994, 98(45), 11733–11738.

[32] G. D. Bromiley, A. A. Shiryaev. Neutron irradiation and post-irradiation annealing of rutile (TiO_{2-x}): Effect on hydrogen incorporation and optical absorption. Phys. Chem. Miner., 2006, 33(6), 426–434.

[33] X. Q. Chen, H. B. Liu, G. B. Gu. Preparation of nanometer crystalline TiO_2 with high photocatalytic activity by pyrolysis of titanyl organic compounds and photocatalytic mechanism. Mater. Chem. Phys., 2005, 91(2–3), 317–324.

[34] X. Wang, Y. Li, X. Liu, S. Gao, B. Huang, Y. Dai. Preparation of Ti^{3+} self-doped TiO_2 nanoparticles and their visible light photocatalytic activity. Chin. J. Catal., 2015, 36, 389–399.

[35] B. Qiu, Y. Zhou, Y. Ma, X. Yang, W. Sheng, M. Xing, J. Zhang. Facile synthesis of the Ti^{3+} self-doped TiO_2-graphene nanosheet composites with enhanced photocatalysis. Sci. Rep., 2015, 5, 8591.

[36] R. Fu, S. Gao, H. Xu, Q. Wang, Z. Wang, B. Huang, Y. Dai. Fabrication of Ti^{3+} self-doped TiO_2(A) nanoparticle/TiO_2(R) nanorod heterojunctions with enhanced visible-light-driven photocatalytic properties. RSC Adv., 2014, 4, 37061–37069.

[37] X. Liu, S. Gao, H. Xu, Z. Lou, W. Wang, B. Huang, Y. Dai. Green synthetic approach for Ti^{3+} self-doped TiO_{2-x} nanoparticles with efficient visible light photocatalytic activity. Nanoscale, 2013, 5, 1870–1875.

[38] X. Xin, T. Xu, J. Yin, L. Wang, C. Wang. Management on the location and concentration of Ti^{3+} in anatase TiO_2 for defects-induced visible-light photocatalysis. Appl. Catal. B Environ., 2015, 176–177, 354–362.

[39] A. Sirisuk, E. Klansorn, P. Praserthdam. Effects of reaction medium and crystallite size on Ti^{3+} surface defects in titanium dioxide nanoparticles prepared by solvothermal method. Catal. Commun., 2008, 9(9), 1810–1814.

[40] L. Si, Z. Huang, K. Lv, D. Tang, C. Yang. Facile preparation of Ti^{3+} self-doped TiO_2 nanosheets with dominant {001} facets using zinc powder as reductant. J. Alloy Compd., 2014, 601, 88–93.

[41] X. Liu, H. Xu, L. R. Grabstanowicz, S. Gao, Z. Lou, W. Wang, B. Huang, Y. Dai, T. Xu. Ti^{3+} self-doped TiO_{2-x} anatase nanoparticles via oxidation of TiH_2 in H_2O_2. Catal. Today, 2014, 225, 80–89.

[42] L. R. Grabstanowicz, S. Gao, T. Li, R. M. Rickard, T. Rajh, D. J. Liu, T. Xu. Facile oxidative conversion of TiH_2 to high-concentration Ti^{3+}-self-doped rutile TiO_2 with visible-light photoactivity. Inorg. Chem., 2013, 52(7), 3884–3890.

[43] J. Tian, X. Hu, H. Yang, Y. Zhou, H. Cui, H. Liu. High yield production of reduced TiO_2 with enhanced photocatalytic activity. Appl. Surf. Sci., 2016, 360, 768–743.

[44] C. Mao, F. Zuo, Y. Hou, X. Bu, P. Feng. *In situ* preparation of a Ti^{3+} self-doped TiO_2 film with enhanced activity as photoanode by N_2H_4 reduction. Angew. Chem. Int. Ed., 2014, 53, 10485–10489.

[45] M. Wen, S. Zhang, W. Dai, G. Li, D. Zhang. *In situ* synthesis of Ti^{3+} self-doped mesoporous TiO_2 as a durable photocatalyst for environmental remediation. Chin. J. Catal., 2015, 36(12), 2095–2102.

[46] Z. He, W. Que, H. Xie, J. Chen, Y. Yuan, P. Sun. Facile synthesis of self-sensitized TiO_2 photocatalysts and their higher photocatalytic activity. J. Am. Ceram. Soc., 2012, 95(12), 3941–3946.

[47] Q. Guo, C. Zhou, Z. Ma, Z. Ren, H. Fan, X. Yang. Elementary photocatalytic chemistry on TiO_2 surfaces. Chem. Soc. Rev., 2016, DOI: 10.1039/c5cs00448a.

[48] S. Wang, X. Yang, Y. Wang, L. Liu, Y. Guo, H. Guo. Morphology-controlled synthesis of Ti^{3+} self-doped yolk–shell structure titanium oxide with superior photocatalytic activity under visible light. J. Solid State Chem., 2014, 213, 98–103.

[49] T. C. Lu, S. Y. Wu, L. B. Lin, W. C. Zheng. Defects in the reduced rutile single crystal. Physica B, 2001, 304(1–4), 147–151.

[50] W. A. Weyl, T. Forland. Photochemistry of rutile. Ind. Eng. Chem., 1950, 42(2), 257–263.

[51] L. B. Xiong, J. L. Li, B. Yang, Y. Yu. Ti^{3+} in the surface of titanium dioxide: Generation, properties and photocatalytic application. J. Nanomater., 2012, 2012, 1–13.

[52] A. S. Bolokang, D. E. Motaung, C. J. Arendse, T. F. G. Muller. Morphology and structural development of reduced anatase-TiO_2 by pure Ti powder upon annealing and nitridation: Synthesis of TiO_x and TiO_xN_y powders. Mater. Charact., 2015, 100, 41–49.

[53] J. Zhang, W. Fu, J. Xi, H. He, S. Zhao, H. Lu, Z. Ji. N-doped rutile TiO_2 nano-rods show tunable photocatalytic selectivity. J. Alloy Compd., 2013, 575, 40–47.

[54] J. Lynch, C. Giannini, J. K. Cooper, A. Loiudice, I. D. Sharp, R. Buonsanti. Substitutional or interstitial site-selective nitrogen doping in TiO_2 nanostructures. J. Phys. Chem. C, 2015, 119(13), 7443–7452.

[55] S. M. El-Sheikh, G. Zhang, H. M. El-Hosainy, A. A. Ismail, K. E. O'Shea, P. Falaras, A. G. Kontos, D. D. Dionysiou. High performance sulfur, nitrogen and carbon doped

mesoporous anatase-brookite TiO_2 photocatalyst for the removal of microcystin-LR under visible light irradiation. J. Hazard. Mater., 2014, 280, 723–733.

[56] J. Yu, G. Dai, Q. Xiang, M. Jaroniec. Fabrication and enhanced visible-light photocatalytic activity of carbon self-doped TiO_2 sheets with exposed {001} facets. J. Mater. Chem., 2011, 21(4), 1049–1057.

[57] V. Štengl, V. Houšková, S. Bakardjieva, N. Murafa. Photocatalytic activity of boron-modified titania under UV and visible-light illumination. ACS Appl. Mater. Inter., 2010, 2(2), 575–580.

[58] X. Wang, M. Blackford, K. Prince, R. A. Caruso. Preparation of boron-doped porous titania networks containing gold nanoparticles with enhanced visible-light photocatalytic activity. ACS Appl. Mater. Inter., 2012, 4(1), 476–482.

[59] N. Patel, A. Dashora, R. Jaiswal, R. Fernandes, M. Yadav, D. C. Kothari, B. L. Ahuja, A. Miotello. Experimental and theoretical investigations on the activity and stability of substitutional and interstitial boron in TiO_2 photocatalyst. J. Phys. Chem. C, 2015, 119(32), 18581–18590.

[60] Z. Li, R. Wnetrzak, W. Kwapinski, J. J. Leahy. Synthesis and characterization of sulfated TiO_2 nanorods and ZrO_2/TiO_2 nanocomposites for the esterification of biobased organic acid. ACS Appl. Mater. Inter., 2012, 4, 4499–4505.

[61] D. Tipayarom, K. Wantala, N. Grisdanurak. Optimization of alachlor degradation on S-doped TiO_2 by sonophotocatalytic activity under visible light. Fresen. Environ. Bull., 2011, 20(6), 1425–1431.

[62] M. Senna, V. Šepelák, J. Shi, B. Bauer, A. Feldhoff, V. Laporte, K. D. Becker. Introduction of oxygen vacancies and fluorine into TiO_2 nanoparticles by co-milling with PTFE. J. Solid State Chem., 2012, 187, 51–57.

[63] A. Kafizas, N. Noor, P. Carmichael, D. O. Scanlon, C. J. Carmalt, I. P. Parkin. Combinatorial atmospheric pressure chemical vapor deposition of $F:TiO_2$: The relationship between photocatalysis and transparent conducting oxide properties. Adv. Funct. Mater., 2014, 24, 1758–1771.

[64] Z. Qiao, S. S. Brown, J. Adcock, G. M. Veith, J. C. Bauer, E. A. Payzant, R. R. Unocic, S. Dai. A topotactic synthetic methodology for highly fluorine-doped mesoporous metal oxides. Angew. Chem. Int. Ed., 2012, 51, 2888–2893.

[65] P. L. Ji, X. Z. Kong, J. G. Wang, X. L. Zhu. Characterization and photocatalytic properties of silver and silver chloride doped TiO_2 hollow nanoparticles. Chin. Chem. Lett., 2012, 23(12), 1399–1402.

[66] H. Xu, Z. Zheng, L. Zhang, H. Zhang, F. Deng. Hierarchical chlorine-doped rutile TiO_2 spherical clusters of nanorods: Large-scale synthesis and high photocatalytic activity. J. Solid State Chem., 2008, 181(9), 2516–2522.

[67] R. Asahi, T. Morikawa, T. Ohwaki, K. Aoki, Y. Taga. Visible-light photocatalysis in nitrogen-doped titanium oxides. Science, 2001, 293, 269–271.

[68] B. Viswanathan, K. R. Krishanmurthy. Nitrogen incorporation in TiO_2: Does it make a visible light photo-active material? Int. J. Photoenergy, 2012, 2012, 1–10.

[69] M. Khan, S. R. Gul, J. Li, W. Cao. Variations in the structural, electronic and optical properties of N-doped TiO_2 with increasing N doping concentration. Mod. Phys. Lett. B, 2015, 29, 1550022.

[70] A. Manole, V. D◎sčaleanu, M. Dobromir, D. Luca. Combining degradation and contact angle data in assessing the photocatalytic TiO_2:N surface. Surf. Interface Anal., 2010, 42(6–7), 947–954.

[71] J. Zhang, Y. Wu, M. Xing, S. Leghari, S. Sajjad. Development of modified N doped TiO_2 photocatalyst with metals, nonmetals and metal oxides. Energ. Environ. Sci., 2010, 3(6), 715–726.

[72] J. Xu, Y. Ao, M. Chen, D. Fu. Photoelectrochemical property and photocatalytic activity of N-doped TiO_2 nanotube arrays. Appl. Surf. Sci., 2010, 256(13), 4397–401.

[73] Z. Lin, A. Orlov, R. M. Lambert, M. C. Payne. New insights into the origin of visible light photocatalytic activity of nitrogen-doped and oxygen-deficient anatase TiO_2. J. Phys. Chem. B, 2005, 109, 20948–20952.

[74] E. M. Samsudin, S. B. A. Hamid, J. C. Juan, W. J. Basirun, A. E. Kandjani, S. K. Bhargava. Controlled nitrogen insertion in titanium dioxide for optimal photocatalytic degradation of atrazine. RSC Adv., 2015, 5, 44041–44052.

[75] H. Y. Ai, J. W. Shi, R. X. Duan, J. W. Chen, H. J. Cui, M. L. Fu. Sol-gel to prepare nitrogen doped TiO_2 nanocrystals with exposed {001} facets and high visible-light photocatalytic performance. Int. J. Photoenergy, 2014, 2014, 1–9.

[76] J. Shi, S. Chen, S. Wang, Z. Ye. Sol-gel preparation and visible light photocatalytic activity of nitrogen doped titania. Procedia Eng., 2012, 27, 564–569.

[77] Q. Gao, Z. Li, M. Li, Y. Liu, C. Song, G. Han. Microstructure and properties of N-doped TiO_2 films grown by dielectric barrier discharge enhanced chemical vapor deposition. J. Mater. Sci. Eng., 2012, 30(1), 93–97.

[78] C. Sarantopoulos, A. N. Gleizes, F. Maury. Chemical vapor deposition and characterization of nitrogen doped TiO_2 thin films on glass substrates. Thin Solid Films, 2009, 518(4), 1299–1303.

[79] K. I. Liu, C. Y. Su, T. P. Perng. Highly porous N-doped TiO_2 hollow fibers with internal three-dimensional interconnected nanotubes for photocatalytic hydrogen production. RSC Adv., 2015, 5, 88367–88374.

[80] H. E. Cheng, Y. R. Chen, W. T. Wu, C. M. Hsu. Effect of nitrogen doping concentration on the properties of TiO_2 films grown by atomic layer deposition. Mater. Sci. Eng. B, 2011, 176(7), 596–599.

[81] L. Tian, A. Soum-Glaude, F. Volpi, L. Salvo, G. Berthomé, S. Coindeau, A. Mantoux, R. Boichot, S. Lay, V. Brizé, E. Blanquet, G. Giusti, D. Bellet. Undoped TiO_2 and nitrogen-doped TiO_2 thin films deposited by atomic layer deposition on planar and architectured surfaces for photovoltaic applications. J. Vac. Sci. Technol. A, 2015, 33, 01A141.

[82] D. H. Wang, L. Jia, X. L. Wu, L. Q. Lu, A. W. Xu. One-step hydrothermal synthesis of N-doped TiO_2/C nanocomposites with high visible light photocatalytic activity. Nanoscale, 2012, 4, 576–584.

[83] B. Buchholcz, H. Haspel, Á. Kukovecz, Z. Kónya. Low-temperature conversion of titanate nanotubes into nitrogen-doped TiO_2 nanoparticles. CrystEngComm, 2014, 16, 7486–7492.

[84] X. Zhang, X. Cui. Facile synthesis of flowery N-doped titanates with enhanced adsorption and photocatalytic performances. RSC Adv., 2014, 4, 60907–60913.

[85] Z. Li, Z. Ren, Y. Qu, S. Du, J. Wu, L. Kong, G. Tian, W. Zhou, H. Fu. Hierarchical N-doped TiO_2 microspheres with exposed (001) facets for enhanced visible light catalysis. Eur. J. Inorg. Chem., 2014, 2146–2152.

[86] J. H. Pan, G. Han, R. Zhou, X. S. Zhao. Hierarchical N-doped TiO_2 hollow microspheres consisting of nanothorns with exposed anatase {101} facets. Chem. Commun., 2011, 47, 6942–6944.

[87] Q. Xiang, J. Yu, W. Wang, M. Jaroniec. Nitrogen self-doped nanosized TiO_2 sheets with exposed {001} facets for enhanced visible-light photocatalytic activity. Chem. Commun., 2011, 47, 6906–6908.

[88] X. Zhou, F. Peng, H. Wang, H. Yu, Y. Fang. A simple preparation of nitrogen doped titanium dioxide nanocrystals with exposed (001) facets with high visible light activity. Chem. Commun., 2012, 48, 600–602.

[89] Y. Luan, L. Jing, M. Xie, X. Shi, X. Fan, Y. Cao, Y. Feng. Synthesis of efficient N-containing TiO_2 photocatalysts with high anatase thermal stability and the effects of the nitrogen residue on the photoinduced charge separation. Phys. Chem. Chem. Phys., 2012, 14, 1352–1359.

[90] X. Cheng, X. Yu, Z. Xing. Characterization and mechanism analysis of N doped TiO_2 with visible light response and its enhanced visible activity. Appl. Surf. Sci., 2012, 258, 3244–3248.

[91] H. Zeng, J. Xie, H. Xie, B. L. Su, M. Wang, H. Ping, W. Wang, H. Wang, Z. Fu. Bioprocess-inspired synthesis of hierarchically porous nitrogen-doped TiO_2 with high visible-light photocatalytic activity. J. Mater. Chem. A, 2015, 3, 19588–19596.

[92] K. Siuzdak, M. Szkoda, M. Sawczaka, A. Lisowska-Oleksiak. Novel nitrogen precursors for electrochemically driven doping of titania nanotubes exhibiting enhanced photoactivity. N. J. Chem., 2015, 39, 2741–2751.

[93] S. Li, S. Lin, J. Liao, N. Pan, D. Li, J. Li. Nitrogen-doped TiO_2 nanotube arrays with enhanced photoelectrochemical property. Int. J. Photoenergy, 2012, 2012, 1–7.

[94] I. Hanzu, T. Djenizian, P. Knauth. Electrical and point defect properties of TiO_2 nanotubes fabricated by electrochemical anodization. J. Phys. Chem. C, 2011, 115(13), 5989–5996.

[95] H. Feng, P. Z. Si, Y. C. Shi, C. H. Jin, X. L. Zhang, J. J. Liu, S. J. Yu, G. H. Zhang, H. L. Ge. Structure and photocatalytic properties of N-doped TiO_{2-x} films prepared by N-ion implantation. Surf. Rev. Lett., 2013, 20, 1350059.

[96] P. Sudhagar, K. Asokan, E. Ito, Y. S. Kang. N-ion-implanted TiO_2 photoanodes in quantum dot-sensitized solar cells. Nanoscale, 2012, 4(7), 2416–2422.

[97] K. Sivaranjani, C. S. Gopinath. Porosity driven photocatalytic activity of wormhole mesoporous $TiO_{2-x}N_x$ in direct sunlight. J. Mater. Chem., 2011, 21, 2639–2647.

[98] J. Huo, Y. Hu, H. Jiang, X. Hou, C. Li. Continuous flame synthesis of near surface nitrogen doped TiO_2 for dye-sensitized solar cells. Chem. Eng. J., 2014, 258, 163–170.

[99] R. A. R. Monteiro, S. M. Miranda, V. J. P. Vilar, L. M. Pastrana-Martínez, P. B. Tavares, R. A. R. Boaventura, J. L. Faria, E. Pinto, A. M. T. Silva. N-modified TiO_2 photocatalytic activity towards diphenhydramine degradation and *Escherichia coli* inactivation in aqueous solutions. Appl. Catal. B Environ., 2015, 162, 66–74.

[100] Y. C. Tang, X. H. Huang, H. Q. Yu, L. H. Tang. Nitrogen-doped photocatalyst prepared by mechanochemical method: Doping mechanisms and visible photoactivity of pollutant degradation. Int. J. Photoenergy, 2012, 2012, 1–10.

[101] R. Rattanakam, S. Supothina. Visible-light-sensitive N-doped TiO_2 photocatalysts prepared by a mechanochemical method: Effect of a nitrogen source. Res. Chem. Intermediat., 2009, 35(3), 263–269.

[102] L. Hu, J. Wang, J. Zhang, Q. Zhang, Z. Liu. An N-doped anatase/rutile TiO_2 hybrid from low-temperature direct nitridization: Enhanced photoactivity under UV-/visible-light. RSC Adv., 2014, 4, 420–427.

[103] H. H. H. Lin, A. Y. C. Lin, C. L. Hung. Photocatalytic oxidation of cytostatic drugs by microwave-treated N-doped TiO_2 under visible light. J. Chem. Technol. Biotechnol., 2015, 90, 1345–1354.

[104] G. Abadias, F. Paumier, D. Eyidi, P. Gúerin, T. Girardeau. Structure and properties of nitrogen-doped titanium dioxide thin films produced by reactive magnetron sputtering. Surf. Interface Anal., 2010, 42, 970–973.

[105] S. Cao, B. Liu, L. Fan, Z. Yue, B. Liu, B. Cao. Highly antibacterial activity of N-doped TiO_2 thin films coated on stainless steel brackets under visible light irradiation. Appl. Surf. Sci., 2014, 309, 119–127.

[106] S. J. Ha, D. H. Kim, J. H. Moon. N-doped mesoporous inverse opal structures for visible-light photocatalysts. RSC Adv., 2015, 5, 77716–77722.

[107] Y. Chen, X. Cao, B. Lin, B. Gao. Origin of the visible-light photoactivity of NH_3-treated TiO_2: Effect of nitrogen doping and oxygen vacancies. Appl. Surf. Sci., 2013, 264, 845–852.

[108] G. Wang, X. Xiao, W. Li, Z. Lin, Z. Zhao, C. Chen, C. Wang, Y. Li, X. Huang, L. Miao, C. Jiang, Y. Huang, X. Duan. Significantly enhanced visible light photoelectrochemical activity in TiO_2 nanowire arrays by nitrogen implantation. Nano Lett., 2015, 15(7), 4692–4698.

[109] X. Jiang, Y. Wang, C. Pan. High concentration substitutional N-doped TiO_2 film: Preparation, characterization, and photocatalytic property. J. Am. Ceram. Soc., 2011, 94(11), 4078–4083.

[110] C. D. Valentin, G. Pacchioni, A. Selloni, S. Livraghi, E. Giamello. Characterization of paramagnetic species in N-doped TiO_2 powders by EPR spectroscopy and DFT calculations. J. Phys. Chem. B, 2005, 109, 11414–11419.

[111] H. Gao, J. Zhou, D. Dai, Y. Qu. Photocatalytic activity and electronic structure analysis of N-doped anatase TiO_2: A combined experimental and theoretical study. Chem. Eng. Technol., 2009, 32(6), 867–872.

[112] A. V. Emeline, V. N. Kuznetsov, V. K. Rybchuk, N. Serpone. Visible-light-active titania photocatalysts: The case of N-doped TiO_2—Properties and some fundamental issues. Int. J. Photoenergy, 2008, 2008, 258394.

[113] H. M. Yates, M. G. Nolan, D. W. Sheel, M. E. J. Pemble. The role of nitrogen doping on the development of visible light-induced photocatalytic activity in thin TiO_2 films grown on glass by chemical vapour deposition. J. Photochem. Photobiol. A, 2006, 179, 213–223.

[114] L. Gai, X. Duan, H. Jiang, Q. Mei, G. Zhou, Y. Tian, H. Liu. One-pot synthesis of nitrogen-doped TiO_2 nanorods with anatase/brookite structures and enhanced photocatalytic activity. CrystEngComm, 2012, 14, 7662–7671.

[115] H. Irie, Y. Watanabe, K. Hashimoto. Nitrogen dependence on photocatalytic activity of $TiO_{2-x}N_x$ powders. J. Phys. Chem. B, 2003, 107, 5483–5486.

[116] Y. T. Lin, C. H. Weng, Y. H. Lin, C. C. Shiesh, F. Y. Chen. Effect of C content and calcination temperature on the photocatalytic activity of C-doped TiO_2 catalyst. Sep. Purif. Technol., 2013, 116, 114–123.

[117] V. Etacheri, G. Michlits, M. K. Seery, S. J. Hinder, S. C. Pillai. A highly efficient $TiO_{2-x}C_x$ nano-heterojunction photocatalyst for visible light induced antibacterial applications. ACS Appl. Mater. Inter., 2013, 5(5), 1663–1672.

[118] F. Cuomo, F. Venditti, A. Ceglie, A. D. Leonardis, V. Macciola, F. Lopez. Cleaning of olive mill wastewaters by visible light activated carbon doped titanium dioxide. RSC Adv., 2015, 5, 85586–85591.

[119] S. U. Khan, M. Al-Shahry, W. B. Ingler. Efficient photochemical water splitting by a chemically modified n-TiO_2. Science 2002, 297, 2243–2245.

[120] J. W. Shi, C. Liu, C. He, J. Li, C. Xie, S. Yang, J. W. Chen, S. Li, C. Niu. Carbon-doped titania nanoplates with exposed {001} facets: Facile synthesis, characterization and visible-light photocatalytic performance. RSC Adv., 2015, 5, 17667–17675.

[121] Y. Zhang, Z. Zhao, J. Chen, L. Cheng, J. Chang, W. Sheng, C. Hu, S. Cao. C-doped hollow TiO_2 spheres: *In situ* synthesis, controlled shell thickness, and superior visible-light photocatalytic activity. Appl. Catal. B Environ., 2015, 165, 715–722.

[122] P. Shao, J. Tian, Z. Zhao, W. Shi, S. Gao, F. Cui. Amorphous TiO_2 doped with carbon for visible light photodegradation of rhodamine B and 4-chlorophenol. Appl. Surf. Sci., 2015, 324, 35–43.

[123] L. Zhang, M. S. Tse, O. K. Tan, Y. X. Wang, M. Han. Facile fabrication and characterization of multi-type carbon-doped TiO_2 for visible light-activated photocatalytic mineralization of gaseous toluene. J. Mater. Chem. A, 2013, 1, 4497–4507.

[124] Y. Yang, D. Ni, Y. Yao, Y. Zhong, Y. Ma, J. Yao. High photocatalytic activity of carbon doped TiO_2 prepared by fast combustion of organic capping ligands. RSC Adv., 2015, 5, 93635–93643.

[125] J. Liu, Q. Zhang, J. Yang, H. Ma, M. O. Tade, S. Wang, J. Liu. Facile synthesis of carbon-doped mesoporous anatase TiO_2 for the enhanced visible-light driven photocatalysis. Chem. Commun., 2014, 50, 13971–13974.

[126] Y. Y. Sun, S. Zhang. Kinetics stabilized doping: Computational optimization of carbon-doped anatase TiO_2 for visible-light driven water splitting. Phys. Chem. Chem. Phys., 2016, 18(4), 2776–2783.

[127] G. Liu, C. Sun, S. C. Smith, L. Wang, G. Q. Lu, H. M. Cheng. Sulfur doped anatase TiO_2 single crystals with a high percentage of {001} facets. J. Colloid Interf. Sci., 2010, 349(2), 477–483.

[128] P. Goswami, J. N. Ganguli. A novel synthetic approach for the preparation of sulfated titania with enhanced photocatalytic activity. RSC Adv., 2013, 3, 8878–8888.

[129] N. Li, X. Zhang, W. Zhou, Z. Liu, G. Xie, Y. Wang, Y. Du. High quality sulfur-doped titanium dioxide nanocatalysts with visible light photocatalytic activity from non-hydrolytic thermolysis synthesis. Inorg. Chem. Front., 2014, 1, 521–525.

[130] P. V. R. K. Ramacharyulu, D. B. Nimbalkar, J. P. Kumar, G. K. Prasad, S. C. Ke. N-doped, S-doped TiO_2 nanocatalysts: Synthesis, characterization and photocatalytic activity in the presence of sunlight. RSC Adv., 2015, 5, 37096–37101.

[131] Y. H. Lin, S. H. Chou, H. Chu. A kinetic study for the degradation of 1,2-dichloroethane by S-doped TiO_2 under visible light. J. Nanopart. Res., 2014, 16(8), 1016–1030.

[132] N. Sharotri, D. Sud. A greener approach to synthesize visible light responsive nanoporous S-doped TiO_2 with enhanced photocatalytic activity. N. J. Chem., 2015, 39, 2217–2223.

[133] J. H. Pan, Z. Cai, Y. Yu, X. S. Zhao. Controllable synthesis of mesoporous F-TiO_2 spheres for effective photocatalysis. J. Mater. Chem., 2011, 21, 11430–11438.

[134] D. Lozano, J. M. Hernández-López, P. Esbrit, M. A. Arenas, E. Gómez-Barrena, J. de Damborenea, J. Esteban, C. Pérez-Jorge, R. Pérez-Tanoira, A. Conde. Influence of the nanostructure of F-doped TiO_2 films on osteoblast growth and function. Soc. Biomater., 2014, 1985–1990.

[135] K. Lv, B. Cheng, J. Yu, G. Liu. Fluorine ions-mediated morphology control of anatase TiO_2 with enhanced photocatalytic activity. Phys. Chem. Chem. Phys., 2012, 14, 5349–5362.

[136] X. K. Wang, C. Wang, W. Q. Jiang, W. L. Guo, J. G. Wang. Sonochemical synthesis and characterization of Cl-doped TiO_2 and its application in the photodegradation of phthalate ester under visible light irradiation. Chem. Eng. J., 2012, 189–190, 288–294.

[137] J. Guo, L. Mao, J. Zhang, C. Feng. Role of Cl^- ions in photooxidation of propylene on TiO_2 surface. Appl. Surf. Sci., 2010, 256(7), 2132–2137.

[138] R. Yuan, T. Chen, E. Fei, J. Lin, Z. Ding, J. Long, Z. Zhang, X. Fu, P. Liu, L. Wu, X. Wang. Surface chlorination of TiO_2-based photocatalysts: A way to remarkably improve photocatalytic activity in both UV and visible region. ACS Catal., 2011, 1(3), 200–206.

[139] H. Lin, W. Deng, T. Zhou, S. Ning, J. Long, X. Wang. Iodine-modified nanocrystalline titania for photocatalytic antibacterial application under visible light illumination. Appl. Catal. B Environ., 2015, 176, 36–43.

[140] D. Wang, X. Li, J. Chen, X. Tao. Enhanced visible-light photoelectrocatalytic degradation of organic contaminants at iodine-doped titanium dioxide film electrode. Ind. Eng. Chem. Res., 2012, 51(1), 218–224.

[141] L. Zhang, J. Zhou, J. Li, G. Liu, X. Lin, B. Mao, R. Liu, S. Zhang, J. Q. Wang. Surface structural reconstruction for optical response in iodine-modified TiO_2 photocatalyst system. J. Phys. Chem. C, 2014, 118(25), 13726–13732.

[142] W. Q. Fang, X. L. Wang, H. Zhang, Y. Jia, Z. Huo, Z. Li, H. Zhao, H. G. Yang, X. Yao. Manipulating solar absorption and electron transport properties of rutile TiO_2 photocatalysts via highly n-type F-doping. J. Mater. Chem. A, 2014, 2, 3513–3520.

[143] R. Rahimi, S. Saadati, E. H. Fard. Fluorine-doped TiO_2 nanoparticles sensitized by tetra(4-carboxyphenyl)porphyrin and zinc tetra(4-carboxyphenyl)porphyrin: Preparation, characterization, and evaluation of photocatalytic activity. Environ. Prog. Sustain. Energ., 2015, 34(5), 1341–1348.

[144] M. V. Dozzi, C. D'Andrea, B. Ohtani, G. Valentini, E. Selli. Fluorine-doped TiO_2 materials: Photocatalytic activity vs time-resolved photoluminescence. J. Phys. Chem. C, 2013, 117(48), 25586–25595.

[145] Y. Wang, H. Zhang, P. Liu, T. Sun, Y. Li, H. Yang, X. Yao, H. Zhao. Nature of visible-light responsive fluorinated titanium dioxides. J. Mater. Chem. A, 2013, 1, 12948–12953.

[146] H. Lin, W. Deng, T. Zhou, S. Ning, J. Long, X. Wang. Iodine-modified nanocrystalline titania for photo-catalytic antibacterial application under visible light illumination. Appl. Catal. B Environ., 2015, 176–177, 36–43.

[147] K. Siuzdak, M. Szkoda, M. Sawczak, A. Lisowska-Oleksiak, J. Karczewski, J. Ryl. Enhanced photoelectrochemical and photocatalytic performance of iodine-doped titania nanotube arrays. RSC Adv., 2015, 5, 50379–50391.

[148] Z. He, L. Xie, J. Tu, S. Song, W. Liu. Visible light-induced degradation of phenol over iodine-doped titanium dioxide modified with platinum: Role of platinum and the reaction mechanism. J. Phys. Chem. C, 2010, 114(1), 526–532.

[149] G. Liu, C. Sun, L. Wang, S. C. Smith, G. Q. Lu, H. M. Cheng. Bandgap narrowing of titanium oxide nanosheets: Homogeneous doping of molecular iodine for improved photoreactivity. J. Mater. Chem., 2011, 21, 14672–14679.

[150] H. Xu, R. A. Picca, L. D. Marco, C. Carlucci, A. Scrascia, P. Papadia, B. F. Scremin, E. Carlino, C. Giannini, C. Malitesta, M. Mazzeo, G. Gigli, G. Ciccarella. Nonhydrolytic route to boron-doped TiO_2 nanocrystals. Eur. J. Inorg. Chem., 2013, (3), 364–374.

[151] T. T. Wu, Y. P. Xie, L. C. Yin, G. Liu, H. M. Cheng. Switching photocatalytic H_2 and O_2 generation preferences of rutile TiO_2 microspheres with dominant reactive facets by boron doping. J. Phys. Chem. C, 2015, 119(1), 84–89.

[152] R. Zheng, Y. Guo, C. Jin, J. Xie, Y. Zhu, Y. Xie. Novel thermally stable phosphorus-doped TiO_2 photocatalyst synthesized by hydrolysis of $TiCl_4$. J. Mol. Catal. A, 2010, 319(1–2), 46–51.

[153] Y. Xia, Y. Jiang, F. Li, M. Xia, B. Xue, Y. Li. Effect of calcined atmosphere on the photocatalytic activity of P-doped TiO_2. Appl. Surf. Sci., 2014, 289, 306–315.

[154] W. Q. Fan, H. Y. Bai, G. H. Zhang, Y. S. Yan, C. B. Liu, W. D. Shi. Titanium dioxide macroporous materials doped with iron: Synthesis and photo-catalytic properties. CrystEngComm, 2014, 16, 116–122.

[155] S. M. Chang, W. S. Liu. The roles of surface-doped metal ions (V, Mn, Fe, Cu, Ce, and W) in the interfacial behavior of TiO_2 photocatalysts. Appl. Catal. B Environ., 2014, 156–157, 466–475.

[156] R. Hahn, M. Stark, M. S. Killian, P. Schmuki. Photocatalytic properties of *in situ* doped TiO_2-nanotubes grown by rapid breakdown anodization. Catal. Sci. Technol., 2013, 3, 1765–1770.

[157] M. Ishii, B. Towlson, S. Harako, X. W. Zhao, S. Komuro, B. Hamilton. Roles of electrons and holes in the luminescence of rare-earth-doped semiconductors. Electr. Commun. Jpn., 2013, 96(11), 1–7.

[158] D. M. Tobaldi, R. C. Pullar, A. F. Gualtieri, M. P. Seabra, J. A. Labrincha. Sol-gel synthesis, characterisation and photocatalytic activity of pure, W-, Ag- and W/Ag co-doped TiO_2 nanopowders. Chem. Eng. J., 2013, 214, 364–375.

[159] J. F. de Lima, M. H. Harunsani, D. J. Martin, D. Kong, P. W. Dunne, D. Gianolio, R. J. Kashtiban, J. Sloan, O. A. Serra, J. Tang, R. I. Walton. Control of chemical state of cerium in doped anatase TiO_2 by solvothermal synthesis and its application in photocatalytic water reduction. J. Mater. Chem. A, 2015, 3, 9890–9898.

[160] H. Li, J. Liu, J. Qian, Q. Li, J. Yang. Preparation of Bi-doped TiO_2 nanoparticles and their visible light photocatalytic performance. Chin. J. Catal., 2014, 35, 1578–1589.

[161] R. Klaysri, S. Wichaidit, T. Tubchareon, S. Nokjan, S. Piticharoenphun, O. Mekasuwandumrong, P. Praserthdam. Impact of calcination atmospheres on the physiochemical and photocatalytic properties of nanocrystalline TiO_2 and Si-doped TiO_2. Ceram. Int., 2015, 41(9), 11409–11417.

[162] Y. Zhao, J. Liu, L. Shi, S. Yuan, J. Fang, Z. Wang, M. Zhang. Solvothermal preparation of Sn^{4+} doped anatase TiO_2 nanocrystals from peroxo-metal-complex and their photocatalytic activity. Appl. Catal. B Environ., 2011, 103(3–4), 436–443.

[163] Y. Zhang, D. S. Kilin. Computational modeling of wet TiO_2 (001) anatase surfaces functionalized by transition metal doping. Int. J. Quantum Chem., 2012, 112(24), 3867–3873.

[164] J. Choi, H. Park, M. R. Hoffmann. Effects of single metal-ion doping on the visible-light photoreactivity of TiO_2. J. Phys. Chem. C, 2010, 114, 783–792.

[165] Y. Ni, Y. Zhu, X. Ma. A simple solution combustion route for the preparation of metal-doped TiO_2 nanoparticles and their photocatalytic degradation properties. Dalton Trans., 2011, 40, 3689–3694.

[166] Q. Meng, T. Wang, E. Liu, X. Ma, Q. Geac, J. Gong. Understanding electronic and optical properties of anatase TiO_2 photocatalysts co-doped with nitrogen and transition metals. Phys. Chem. Chem. Phys., 2013, 15(24), 9549–9561.

[167] Y. F. Zhao, C. Li, S. Lu, L. J. Yan, Y. Y. Gong, L. Y. Niu, X. J. Liu. Effects of oxygen vacancy on 3*d* transition-metal doped anatase TiO_2: First principles calculations. Chem. Phys. Lett., 2016, 647, 36–41.

[168] S. Manu, M. A. Khadar. Non-uniform distribution of dopant iron ions in TiO_2 nanocrystals probed by X-ray diffraction, Raman scattering, photoluminescence and photocatalysis. J. Mater. Chem. C, 2015, 3, 1846–1853.

[169] J. Yan, Y. Zhang, S. Liu, G. Wu, L. Li, N. Guan. Facile synthesis of an iron doped rutile TiO_2 photocatalyst for enhanced visible-light-driven water oxidation. J. Mater. Chem. A, 2015, 3, 21434–21438.

[170] T. Liu, H. Zhang. Novel Fe-doped anatase TiO_2 nanosheet hierarchical spheres with 94% {001} facets for efficient visible light photodegradation of organic dye. RSC Adv., 2013, 3, 16255–16258.

[171] R. M. Ramli, F. K. Chong, A. A. Omar, T. Murugesan. Performance of surfactant assisted synthesis of Fe/TiO_2 on the photodegradation of diisopropanolamine. Clean Soil Air Water, 2015, 43 (5), 690–697.

[172] Y. Su, Z. Wu, Y. Wu, J. Yu, L. Sun, C. Lin. Acid orange II degradation through a heterogeneous Fenton-like reaction using Fe-TiO_2 nanotube arrays as a photocatalyst. J. Mater. Chem. A, 2015, 3, 8537–8544.

[173] G. K. Dinesh, S. Anandan, T. Sivasankar. Sonophotocatalytic treatment of Bismarck Brown G dye and real textile effluent using synthesized novel Fe(0)-doped TiO_2 catalyst. RSC Adv., 2015, 5, 10440–10451.

[174] D. Flak, E. Coy, G. Nowaczyk, L. Yate, S. Jurga. Tuning the photodynamic efficiency of TiO_2 nanotubes against HeLa cancer cells by Fe-doping. RSC Adv., 2015, 5, 85139–85152.

[175] R. Su, R. Bechstein, J. Kibsgaard, R. T. Vang, F. Besenbacher. High-quality Fe-doped TiO_2 films with superior visible-light performance. J. Mater. Chem., 2012, 22, 23755–23758.

[176] S. Wang, J. S. Lian, W. T. Zheng, Q. Jiang. Photocatalytic property of Fe doped anatase and rutile TiO_2 nanocrystal particles prepared by sol-gel technique. Appl. Surf. Sci., 2012, 263(15), 260–265.

[177] X. Li, Z. Guo, T. He. The doping mechanism of Cr into TiO_2 and its influence on the photocatalytic performance. Phys. Chem. Chem. Phys., 2013, 15, 20037–20045.

[178] J. M. Herrmann. Detrimental cationic doping of titania in photocatalysis: Why chromium Cr^{3+}-doping is a catastrophe for photocatalysis, both under UV- and visible irradiations. N. J. Chem., 2012, 36, 883–890.

[179] S. Ould-Chikh, O. Proux, P. Afanasiev, L. Khrouz, M. N. Hedhili, D. H. Anjum, M. Harb, C. Geantet, J. M. Basset, E. Puzenat. Photocatalysis with chromium-doped TiO_2: Bulk and surface doping. ChemSusChem, 2014, 7(5), 1361–1371.

[180] C. Diaz-Uribe, W. Vallejo, W. Ramos. Methylene blue photocatalytic mineralization under visible irradiation on TiO_2 thin films doped with chromium. Appl. Surf. Sci., 2014, 319, 121–127.

[181] B. N. Joshi, H. Yoon, M. F. A. M. van Hest, S. S. Yoon. Niobium-doped titania photocatalyst film prepared via a nonaqueous sol-gel method. J. Am. Ceram. Soc., 2013, 96(8), 2623–2627.

[182] P. S. Archana, R. Jose, T. M. Jin, C. Vijila, M. M. Yusoff, S. Ramakrishna. Structural and electrical properties of Nb-doped anatase TiO_2 nanowires by electrospinning. J. Am. Ceram. Soc., 2010, 93(12), 4096–4102.

[183] P. S. Archana, R. Jose, M. M. Yusoff, S. Ramakrishna. Near band-edge electron diffusion in electrospun Nb-doped anatase TiO_2 nanofibers probed by electrochemical impedance spectroscopy. Appl. Phys. Lett., 2011, 98(15), 152103.

[184] J. Yang, X. Zhang, C. Wang, P. Sun, L. Wang, B. Xia, Y. Liu. Solar photocatalytic activities of porous Nb-doped TiO_2 microspheres prepared by ultrasonic spray pyrolysis. Solid State Sci., 2012, 14(1), 139–144.

[185] J. Liu, X. Zhao, L. Duan, M. Cao, H. Sun, J. Shao, S. Chen, H. Xie, X. Chang, C. Chen. Influence of annealing process on conductive properties of Nb-doped TiO_2 polycrystalline films prepared by sol-gel method. Appl. Surf. Sci., 2011, 257(23), 10156–10160.

[186] S. Wang, X. Zhang, D. Ma, Z. Yu, X. Wang, Y. Niu. Photocatalysis performance of Nb-doped TiO_2 film *in situ* growth prepared by a micro plasma method. Rare Metal Mater. Eng., 2014, 43(7), 1549–1552.

[187] S. Liu, E. Guo, L. Yin. Tailored visible-light driven anatase TiO_2 photocatalysts based on controllable metal ion doping and ordered mesoporous structure. J. Mater. Chem., 2012, 22, 5031–5041.

[188] E. O. Oseghe, P. G. Ndungu, S. B. Jonnalagadda. Photocatalytic degradation of 4-chloro-2-methylphenoxyacetic acid using W-doped TiO_2. J. Photochem. Photobiol. A, 2015, 312, 96–106.

[189] W. Sangkhun, L. Laokiat, V. Tanboonchuy, P. Khamdahsag, N. Grisdanurak. Photocatalytic degradation of BTEX using W-doped TiO_2 immobilized on fiber glass cloth under visible light. Superlattice Microst., 2012, 52, 632–642.

[190] A. Mayoufi, M. F. Nsib, A. Houas. Doping level effect on visible-light irradiation W-doped TiO_2-anatase photocatalysts for Congo red photodegradation. C. R. Chimie, 2014, 17(7–8), 818–823.

[191] E. Grabowska, J. W. Sobczak, M. Gazda, A. Zaleska. Surface properties and visible light activity of W-TiO_2 photocatalysts prepared by surface impregnation and sol-gel method. Appl. Catal. B Environ., 2012, 117–118, 351–359.

[192] F. Zhang, Z. Cheng, L. Kang, L. Cui, W. Liu, X. Xu, G. Hou, H. Yang. A novel preparation of Ag-doped TiO_2 nanofibers with enhanced stability of photocatalytic activity. RSC Adv., 2015, 5, 32088–32091.

[193] L. M. Santos, W. A. Machado, M. D. França, K. A. Borges, R. M. Paniago, A. O. T. Patrocinio, A. E. H. Machado. Structural characterization of Ag-doped TiO_2 with enhanced photocatalytic activity. RSC Adv., 2015, 5, 103752–103759.

[194] A. M. A. Abdel-Wahab, O. S. Mohamed, S. A. Ahmed, M. F. Mostafa. Ag-doped TiO_2 enhanced photocatalytic oxidation of 1,2-cyclohexanediol. J. Phys. Org. Chem., 2012, 25, 1418–1421.

[195] A. López Ortiz, M. Meléndez Zaragoza, J. Salinas Gutiérrez, M. M. da Silva Paula, V. Collins-Martínez. Silver oxidation state effect on the photocatalytic properties of Ag doped TiO_2 for hydrogen production under visible light. Int. J. Hydrogen Energ., 2015, 40(48), 17308–17315.

[196] R. Nainan, P. Thakur, M. Chaskar. Synthesis of silver doped TiO_2 nanoparticles for the improved photocatalytic degradation of methyl orange. J. Mater. Sci. Technol., 2012, 1, 52–58.

[197] K. Gupta, R. P. Singh, A. Pandey, P. Anjana. Photocatalytic antibacterial performance of TiO_2 and Ag-doped TiO_2 against *S. aureus. P. aeruginosa* and *E. coli*. Beilstein J. Nanotechnol., 2013, 4, 345–351.

[198] S. Sajjad, S. A. K. Leghari, J. Zhang. Copper impregnated ionic liquid assisted mesoporous titania: Visible light photocatalyst. RSC Adv., 2013, 3, 12678–12687.

[199] X. J. Yang, S. Wang, H. M. Sun, X. B. Wang, J. S. Lian. Preparation and photocatalytic performance of Cu-doped TiO_2 nanoparticles. Trans. Nonferrous Met. Soc. China, 2015, 25, 504–509.

[200] C. Zhao, X. Shu, D. C. Zhu, S. H. Wei, Y. X. Wang, M. J. Tu, W. Gao. High visible light photocatalytic property of Co^{2+}-doped TiO_2 nanoparticles with mixed phases. Superlattice Microst., 2015, 88, 32–42.

[201] I. Ganesh, A. K. Gupta, P. P. Kumar, P. S. C. Sekhar, K. Radha, G. Padmanabham, G. Sundararajan. Preparation and characterization of Co-doped TiO_2 materials for solar light induced current and photocatalytic applications. Mater. Chem. Phys., 2012, 135(1), 220–234.

[202] L. Cai, I. S. Cho, M. Logar, A. Mehta, J. He, C. H. Lee, P. M. Rao, Y. Feng, J. Wilcox, F. B. Prinz, X. Zheng. Sol-flame synthesis of cobalt-doped TiO_2 nanowires with enhanced electrocatalytic activity for oxygen evolution reaction. Phys. Chem. Chem. Phys., 2014, 16, 12299–12306.

[203] A. Sengele, D. Robert, N. Keller, V. Keller, A. Herissan, C. Colbeau-Justin. Ta-doped TiO_2 as photocatalyst for UV: A activated elimination of chemical warfare agent simulant. J. Catal., 2016, 334, 129–141.

[204] S. M. Bawaked, S. Sathasivam, D. S. Bhachu, N. Chadwick, A. Y. Obaid, S. Al-Thabaiti, S. N. Basahel, C. J. Carmalt, I. P. Parkin. Aerosol assisted chemical vapor deposition of conductive and photocatalytically active tantalum doped titanium dioxide films. J. Mater. Chem. A, 2014, 2, 12849–12856.

[205] L. R. Sheppard, J. Holik, R. Liu, S. Macartney, R. Wuhrer. Tantalum enrichment in tantalum-doped titanium dioxide. J. Am. Ceram. Soc., 2014, 97(12), 3793–3799.

[206] J. Majeed, C. Nayak, S. N. Jha, K. Bhattacharyya, D. Bhattacharyy, A. K. Tripathi. Correlation of Mo dopant and photocatalytic properties of Mo incorporated TiO_2: An EXAFS and photocatalytic study. RSC Adv., 2015, 5, 90932–90940.

[207] J. Q. Li, D. F. Wang, H. Liu, Z. F. Zhu. Multilayered Mo-doped TiO_2 nanofibers and enhanced photocatalytic activity. Mater. Manuf. Process., 2012, 27(6), 631–635.

[208] S. Wang, L. N. Bai, H. M. Sun, Q. Jiang, J. S. Lian. Structure and photocatalytic property of Mo-doped TiO_2 nanoparticles. Powder Technol., 2013, 244, 9–15.

[209] S. K. M. Saad, A. A. Umar, H. Q. Nguyen, C. F. Dee, M. M. Salleh, M. Oyama. Porous (001)-faceted Zn-doped anatase TiO_2 nanowalls and their heterogeneous photocatalytic characterization. RSC Adv., 2014, 4, 57054–57063.

[210] M. Sanchez-Dominguez, G. Morales-Mendoza, M. J. Rodriguez-Vargas, C. C. Ibarra-Malo, A. A. Rodriguez-Rodriguez, A. V. Vela-Gonzalez, S. A. Perez-Garcia, R. Gomez. Synthesis of Zn-doped TiO_2 anoparticles by the novel oil-in-water (O/W) microemulsion method and their use for the photocatalytic degradation of phenol. J. Environ. Chem. Eng., 2015, 3(4), 3037–3047.

[211] Y. Wang, X. Xue, H. Yang. Modification of the antibacterial activity of Zn/TiO_2 nanomaterials through different anions doped. Vacuum, 2014, 101, 193–199.

[212] H. Hu, W. Zhang, Y. Qiao, X. Jiang, X. Liu, C. Ding. Antibacterial activity and increased bone marrow stem cell functions of Zn-incorporated TiO_2 coatings on titanium. Acta Biomater., 2012, 8, 904–915.

[213] C. M. Malengreaux, S. L. Pirard, J. R. Bartlett, B. Heinrichs. Kinetic study of 4-nitrophenol photocatalytic degradation over a Zn^{2+} doped TiO_2 catalyst prepared through an environmentally friendly aqueous sol-gel process. Chem. Eng. J., 2014, 245, 180–190.

[214] V. D. Binasa, K. Sambani, T. Maggosc, A. Katsanaki, G. Kiriakidis. Synthesis and photocatalytic activity of Mn-doped TiO_2 nanostructured powders under UV and visible light. Appl. Catal. B Environ., 2012, 113–114, 79–86.

[215] V. C. Papadimitriou, V. G. Stefanopoulos, M. N. Romanias, P. Papagiannakopoulos, K. Sambani, V. Tudose, G. Kiriakidis. Determination of photo-catalytic activity of un-

doped and Mn-doped TiO_2 anatase powders on acetaldehyde under UV and visible light. Thin Solid Films, 2011, 520, 1195–1201.

[216] M. E. Olya, A. Pirkarami, M. Soleimani, M. Bahmaei. Photoelectrocatalytic degradation of acid dye using Ni-TiO_2 with the energy supplied by solar cell: Mechanism and economical studies. J. Environ. Manage., 2013, 121, 210–219.

[217] C. Y. Chen, L. J. Hsu. Kinetic study of self-assembly of Ni(II)-doped TiO_2 nanocatalysts for the photodegradation of azo pollutants. RSC Adv., 2015, 5(107), 88266–88271.

[218] R. Vasilić, S. Stojadinović, N. Radić, P. Stefanov, Z. Dohčević-Mitrović, B. Grbić. One-step preparation and photocatalytic performance of vanadium doped TiO_2 coatings. Mater. Chem. Phys., 2015, 151, 337–344.

[219] M. Khan, Y. Song, N. Chen, W. Cao. Effect of V doping concentration on the electronic structure, optical and photocatalytic properties of nano-sized V-doped anatase TiO_2. Mater. Chem. Phys., 2013, 142(1), 148–153.

[220] W. Li. Influence of electronic structures of doped TiO_2 on their photocatalysis. Phys. Status Solidi R, 2014, 1–18.

[221] E. L. Boulbar, E. Millon, C. Boulmer-Leborgne, C. Cachoncinlle, B. Hakim, E. Ntsoenzok. Optical properties of rare earth-doped TiO_2 anatase and rutile thin films grown by pulsed-laser deposition. Thin Solid Films, 2014, 553, 13–16.

[222] Y. T. Ma, S. D. Li. Photocatalytic activity of TiO_2 nanofibers with doped La prepared by electrospinning method. J. Chin. Chem. Soc., 2015, 62, 380–384.

[223] M. Borlaf, M. T. Colomer, A. de Andrés, F. Cabello, R. Serna, R. Moreno. TiO_2/Eu^{3+} thin films with high photoluminescence emission prepared by electrophoretic deposition from nanoparticulate sols. Eur. J. Inorg. Chem., 2014, 5152–5159.

[224] J. Du, B. Li, J. Huang, W. Zhang, H. Peng, J. Zou. Hydrophilic and photocatalytic performances of lanthanum doped titanium dioxide thin films. J. Rare Earth, 2013, 31(10), 992–996.

[225] S. Han, R. Deng, X. Xie, X. Liu. Enhancing luminescence in lanthanide-doped upconversion nanoparticles. Angew. Chem. Int. Ed., 2014, 53, 11702–11715.

[226] S. Maddila, E. O. Oseghe, S. B. Jonnalagadda. Photocatalyzed ozonation by Ce doped TiO_2 catalyst degradation of pesticide Dicamba in water. J. Chem. Technol. Biotechnol., 2016, 91(2), 385–393.

[227] J. Santiago-Morales, A. Agüera, M. del Mar Gómez, A. R. Fernández-Alba, J. Giménez, S. Esplugas, R. Rosal. Transformation products and reaction kinetics in simulated solar light photocatalytic degradation of propranolol using Ce-doped TiO_2. Appl. Catal. B Environ., 2013, 129, 13–29.

[228] B. Choudhury, B. Borah, A. Choudhury. Extending photocatalytic activity of TiO_2 nanoparticles to visible region of illumination by doping of cerium. Photochem. Photobiol., 2012, 88, 257–264.

[229] Z. Shi, M. Zhou, D. Zheng, H. Liu, S. Yao. Preparation of Ce-doped TiO_2 hollow fibers and their photocatalytic degradation properties for dye compound. J. Chin. Chem. Soc., 2013, 60, 1156–1162.

[230] W. Luo, C. Fu, R. Li, Y. Liu, H. Zhu, X. Chen. Er^{3+}-doped anatase TiO_2 nanocrystals: Crystal-field levels, excited-state dynamics, upconversion, and defect luminescence. Small, 2011, 7(21), 3046–3056.

[231] S. Obregon, G. Colon. Evidence of upconversion luminescence contribution to the improved photoactivity of erbium doped TiO_2 systems. Chem. Commun., 2012, 48, 7865–7867.

[232] Y. Zheng, W. Wang. Electrospun nanofibers of Er^{3+}-doped TiO_2 with photocatalytic activity beyond the absorption edge. J. Solid State Chem., 2014, 210, 206–212.

[233] J. Choi, P. Sudhagar, P. Lakshmipathiraj, J. W. Lee, A. Devadoss, S. Lee, T. Song, S. Hong, S. Eito, C. Terashima, T. H. Han, J. K. Kang, A. Fujishima, Y. S. Kang, U. Paik. Three-dimensional Gd-doped TiO_2 fibrous photoelectrodes for efficient visible light-driven photocatalytic performance. RSC Adv., 2014, 4, 11750–11757.

[234] C. M. Leroy, H. F. Wang, A. Fargues, T. Cardinal, V. Jubera, M. Treguer-Delapierre, C. Boissière, D. Grosso, C. Sanchez, B. Viana, F. Pelle. Emission-photoactivity cross-processing of mesoporous interfacial charge transfer in Eu^{3+} doped titania. Phys. Chem. Chem. Phys., 2011, 13, 11878–11884.

[235] A. Mezzi, S. Kaciulis, I. Cacciotti, A. Bianco, G. Gusmano, F. R. Lamastra, M. E. Fragal. Structure and composition of electrospun titania nanofibres doped with Eu. Surf. Interface Anal., 2010, 42, 572–575.

[236] H. Zhang, Y. Sheng, K. Zheng, X. Zhou, Z. Shi, X. Xu, H. Zou. Hydrothermal fabrication and luminescence properties of one-dimensional TiO_2: Eu^{3+} spindlelike nanorods. Eur. J. Inorg. Chem., 2014, 3305–3311.

[237] Y. Wu, Q. Zhang, X. Yin, H. Cheng. Template-free synthesis of mesoporous anatase yttrium-doped TiO_2 nanosheet-array films from waste tricolor fluorescent powder with high photocatalytic activity. RSC Adv., 2013, 3, 9670–9676.

[238] Z. X. Li, F. B. Shi, T. Zhang, H. S. Wu, L. D. Sun, C. H. Yan. Ytterbium stabilized ordered mesoporous titania for near-infrared photocatalysis. Chem. Commun., 2011, 47, 8109–8111.

[239] C. Spreafico, J. V. Vondele. Excess electrons and interstitial Li atoms in TiO_2 anatase: Properties of the (101) interface. J. Phys. Chem. C, 2015, 119(27), 15009–15018.

[240] S. Bouattour, W. Kallel, A. B. do Rego, L. F. V. Ferreira, I. F. Machado, S. Boufi. Li-doped nanosized TiO_2 powder with enhanced photocatalytic activity under sunlight irradiation. Appl. Organometal. Chem., 2010, 24, 692–699.

[241] W. Yue, C. Randorn, P. S. Attidekou, Z. Su, J. T. S. Irvine, W. Zhou. Syntheses, Li insertion, and photoactivity of mesoporous crystalline TiO_2. Adv. Funct. Mater., 2009, 19, 2826–2833.

[242] R. Long, Y. Dai, G. Meng, B. B. Huang. Energetic and electronic properties of X-(Si, Ge, Sn, Pb) doped TiO_2 from first-principles. Phys. Chem. Chem. Phys., 2009, 11, 8165–8172.

[243] M. C. Wu, J. S. Chih, W. K. Huang. Bismuth doping effect on TiO_2 nanofibres for morphological change and photocatalytic performance. CrystEngComm, 2014, 16, 10692–10699.

[244] W. Zhao, X. Wang, H. Sang, K. Wang. Synthesis of Bi-doped TiO_2 nanotubes and enhanced photocatalytic activity for hydrogen evolution from glycerol solution. Chin. J. Chem., 2013, 31, 415–420.

[245] S. Murcia-López, M. C. Hidalgo, J. A. Navío. Synthesis, characterization and photocatalytic activity of Bi-doped TiO_2 photocatalysts under simulated solar irradiation. Appl. Catal. A Gen., 2011, 404(1–2), 59–67.

[246] F. E. Oropeza, B. Davies, R. G. Palgrave, R. G. Egdell. Electronic basis of visible region activity in high area Sn-doped rutile TiO_2 photocatalysts. Phys. Chem. Chem. Phys., 2011, 13, 7882–7891.

[247] J. Du, G. Zhao, H. Pang, Y. Qian, H. Liu, D. J. Kang. A template method for synthesis of porous Sn-doped TiO_2 monolith and its enhanced photocatalytic activity. Mater. Lett., 2013, 93, 419–422.

[248] J. A. Rengifo-Herrera, K. Pierzchała, A. Sienkiewicz, L. Forró, J. Kiwi, J. E. Moser, C. Pulgarin. Synthesis, characterization, and photocatalytic activities of nanoparticulate N, S-codoped TiO_2 having different surface-to-volume ratios. J. Phys. Chem. C, 2010, 114, 2717–2723.

[249] C. Yu, D. Cai, K. Yang, J. C. Yu, Y. Zhou, C. Fan. Sol-gel derived S, I-codoped mesoporous TiO_2 photocatalyst with high visible-light photocatalytic activity. J. Phys. Chem. Solids, 2010, 71, 1337–1343.

[250] Q. C. Xu, D. V. Wellia, S. Yan, D. W. Liao, T. M. Lim, T. T. Y. Tan. Enhanced photocatalytic activity of C-N-codoped TiO_2 films prepared via an organic-free approach. J. Hazard. Mater., 2011, 188, 172–180.

[251] J. Zhang, C. Pan, P. Fang, J. Wei, R. Xiong. Mo plus C codoped TiO_2 using thermal oxidation for enhancing photocatalytic activity. ACS Appl. Mater. Inter., 2010, 2(4), 1173–1176.

[252] Y. Zhang, C. Li, C. Pan. N plus Ni codoped anatase TiO_2 nano-crystals with exposed {001} facets through two-step hydrothermal route. J. Am. Ceram. Soc., 2012, 95(9), 2951–2956.

[253] X. Li, Y. Liu, P. Yang, Y. Shi. Visible light-driven photocatalysis of W, N co-doped TiO_2. Particuology, 2013, 11, 732–736.

[254] F. Li, L. X. Guan, M. L. Dai, J. J. Feng, M. M. Yao. Effects of V and Zn codoping on the microstructures and photocatalytic activities of nanocrystalline TiO_2 films. Ceram. Int., 2013, 39(7), 7395–7400.

[255] W. F. Chen, P. Koshy, C. C. Sorrell. Effect of intervalence charge transfer on photocatalytic performance of cobalt- and vanadium-codoped TiO_2 thin films. Int. J. Hydrogen Energ., 2015, 40(46), 16215–16229.

[256] Y. Wang, Y. Zhang, F. Yu, C. Jin, X. Liu, J. Ma, Y. Wang, Y. Huang, J. Wang. Correlation investigation on the visible-light-driven photocatalytic activity and coordination structure of rutile Sn-Fe-TiO_2 nanocrystallites for methylene blue degradation. Catal. Today, 2015, 258, 112–119.

[257] J. Chung, J. W. Chung, S. Y. Kwak. Adsorption-assisted photocatalytic activity of nitrogen and sulfur codoped TiO_2 under visible light irradiation. Phys. Chem. Chem. Phys., 2015, 17, 17279–17287.

[258] S. Pany, K. M. Parida. Sulfate-anchored hierarchical meso-macroporous N-doped TiO_2: A novel photocatalyst for visible light H_2 evolution. ACS Sustain. Chem. Eng., 2014, 2(6), 1429–1438.

[259] Z. Li, Y. Zhu, F. Pang, H. Liu, X. Gao, W. Ou, J. Liu, X. Wang, X. Cheng, Y. Zhang. Synthesis of N doped and N, S co-doped 3D TiO_2 hollow spheres with enhanced photocatalytic efficiency under nature sunlight. Ceram. Int., 2015, 41(8), 10063–10069.

[260] V. Etacheri, M. K. Seery, S. J. Hinder, S. C. Pillai. Nanostructured $Ti_{1-x}S_xO_{2-y}N_y$ heterojunctions for efficient visible-light-induced photocatalysis. Inorg. Chem., 2012, 51(13), 7164–7173.

[261] Q. Xiang, J. Yu, M. Jaroniec. Nitrogen and sulfur co-doped TiO_2 nanosheets with exposed {001} facets: Synthesis, characterization and visible-light photocatalytic activity. Phys. Chem. Chem. Phys., 2011, 13, 4853–4861.

[262] E. M. Samsudin, S. B. A. Hamid, J. C. Juan, W. J. Basirun, G. Centi. Enhancement of the intrinsic photocatalytic activity of TiO_2 in the degradation of 1,3,5-triazine herbicides by doping with N, F. Chem. Eng. J., 2015, 280, 330–343.

[263] T. K. Rahul, N. Sandhyarani. Nitrogen-fluorine co-doped titania inverse opals for enhanced solar light driven photocatalysis. Nanoscale, 2015, 7, 18259–18270.

[264] X. Wang, X. Wang, J. Zhao, J. Chen, J. Zhang, J. Song, J. Huang. Bioframe synthesis of NF-TiO_2/straw charcoal composites for enhanced adsorption-visible light photocatalytic degradation of RhB. RSC Adv., 2015, 5, 66611–66620.

[265] A. E. Giannakas, E. Seristatidou, Y. Deligiannakis, I. Konstantinou. Photocatalytic activity of N-doped and N-F co-doped TiO_2 and reduction of chromium(VI) in aqueous solution: An EPR study. Appl. Catal. B Environ., 2013, 132–133, 460–468.

[266] X. Zong, Z. Xing, H. Yu, Z. Chen, F. Tang, J. Zou, G. Q. Lu, L. Wang. Photocatalytic water oxidation on F, N co-doped TiO_2 with dominant exposed {001} facets under visible light. Chem. Commun., 2011, 47, 11742–11744.

[267] A. G. Kontos, M. Pelaez, V. Likodimos, N. Vaenas, D. D. Dionysiou, P. Falaras. Visible light induced wetting of nanostructured N-F co-doped titania films. Photochem. Photobiol. Sci., 2011, 10, 350–354.

[268] A. M. Czoska, S. Livraghi, M. C. Paganini, E. Giamello, C. Di Valentin, G. Pacchioni. The nitrogen-boron paramagnetic center in visible light sensitized N-B co-doped TiO_2: Experimental and theoretical characterization. Phys. Chem. Chem. Phys., 2011, 13, 136–143.

[269] X. Wang, W. Wang, X. Wang, J. Zhang, Z. Gu, L. Zhou, J. Zhao. Enhanced visible light photocatalytic activity of a floating photocatalyst based on B-N-codoped TiO_2 grafted on expanded perlite. RSC Adv., 2015, 5, 41385–41392.

[270] K. Zhang, X. Wang, T. He, X. Guo, Y. Feng. Preparation and photocatalytic activity of B-N co-doped mesoporous TiO_2. Powder Technol., 2014, 253, 608–613.

[271] X. Liu, Y. Chen, C. Cao, J. Xu, Q. Qian, Y. Luo, H. Xue, L. Xiao, Y. Chenac, Q. Chen. Electrospun nitrogen and carbon co-doped porous TiO_2 nanofibers with high visible light photocatalytic activity. N. J. Chem., 2015, 39, 6944–6950.

[272] L. Li, J. Shi, G. Li, Y. Yuan, Y. Li, W. Zhao, J. Shi. One-pot pyrolytic synthesis of C-N-codoped mesoporous anatase TiO_2 and its highly efficient photo-degradation properties. N. J. Chem., 2013, 37, 451–457.

[273] S. Wei, R. Wu, J. Jian, F. Chen, Y. Sun. Black and yellow anatase titania formed by (H, N)-doping: Strong visible-light absorption and enhanced visible-light photocatalysis. Dalton Trans., 2015, 44, 1534–1538.

[274] H. Pan, Y. W. Zhang, V. B. Shenoy, H. Gao. Effects of H-, N-, and (H, N)-doping on the photocatalytic activity of TiO_2. J. Phys. Chem. C, 2011, 115(24), 12224–12231.

[275] J. Yu, P. Zhou, Q. Li. New insight into the enhanced visible-light photocatalytic activities of B-, C- and B/C-doped anatase TiO_2 by first-principles. Phys. Chem. Chem. Phys., 2013, 15, 12040–12047.

[276] Y. Lin, Z. Jiang, C. Zhu, X. Hu, X. Zhang, H. Zhu, J. Fand, S. H. Lin. C/B codoping effect on band gap narrowing and optical performance of TiO_2 photocatalyst: A spin-polarized DFT study. J. Mater. Chem. A, 2013, 1, 4516–4524.

[277] Q. Deng, Y. Liu, K. Mu, Y. Zeng, G. Yang, F. Shen, S. Deng, X. Zhang, Y. Zhang. Preparation and characterization of F-modified C-TiO_2 and its photocatalytic properties. Phys. Status Solidi A, 2015, 212(3), 691–697.

[278] P. Xu, T. Xu, J. Lu, S. Gao, N. S. Hosmane, B. Huang, Y. Dai, Y. Wang. Visible-light-driven photocatalytic S- and C- codoped meso/nanoporous TiO_2. Energ. Environ. Sci., 2010, 3, 1128–1134.

[279] S. Yu, B. Li, Y. Luo, L. Dong, M. Fan, F. Zhang. Preparation of Ag-modified (B, P)-codoped TiO_2 hollow spheres with enhanced photocatalytic activity. Eur. J. Inorg. Chem., 2014, 1142–1149.

[280] H. Li, J. Xing, Z. Xia, J. Chen. Preparation of extremely smooth and boron-fluorine co-doped TiO_2 nanotube arrays with enhanced photoelectrochemical and photocatalytic performance. Electrochim. Acta, 2014, 139, 331–336.

[281] R. Ramanathan, V. Bansal. Ionic liquid mediated synthesis of nitrogen, carbon and fluorine-codoped rutile TiO_2 nanorods for improved UV and visible light photocatalysis. RSC Adv., 2015, 5, 1424–1429.

[282] A. E. Giannakas, M. Antonopoulou, C. Daikopoulos, Y. Deligiannakis, I. Konstantinou. Characterization and catalytic performance of B-doped, B-N co-doped and B-N-F tri-doped TiO_2 towards simultaneous Cr(VI) reduction and benzoic acid oxidation. Appl. Catal. B Environ., 2016, 184, 44–54.

[283] J. Yu, Q. Li, S. Liu, M. Jaroniec. Ionic-liquid-assisted synthesis of uniform fluorinated B/C-codoped TiO_2 nanocrystals and their enhanced visible-light photocatalytic activity. Chem. Eur. J., 2013, 19, 2433–2441.

[284] G. Zhang, Y. C. Zhang, M. Nadagouda, C. Han, K. O'Shea, S. M. El-Sheikh, A. A. Ismail, D. D. Dionysiou. Visible light-sensitized S, N and C co-doped polymorphic TiO_2 for photocatalytic destruction of microcystin-LR. Appl. Catal. B Environ., 2014, 144, 614–621.

[285] H. Zhang, Z. Xing, Y. Zhang, Z. Li, X. Wu, C. Liu, Q. Zhu, W. Zhou. Ni^{2+} and Ti^{3+} co-doped porous black anatase TiO_2 with unprecedented-high visible-light-driven photocatalytic degradation performance. RSC Adv., 2015, 5, 107150–107157.

[286] B. Chen, A. J. Haring, J. A. Beach, M. Li, G. S. Doucette, A. J. Morris, R. B. Moore, S. Priya. Visible light induced photocatalytic activity of Fe^{3+}/Ti^{3+} co-doped TiO_2 nanostructures. RSC Adv., 2014, 4, 18033–18037.

[287] M. Khan, S. R. Gul, J. Li, W. Cao. Tungsten concentration influence on the structural, electronic, optical and photocatalytic properties of tungsten-silver codoped titanium dioxide. Ceram. Int., 2015, 41(4), 6051–6054.

[288] H. F. Moafi, A. F. Shojaie, M. A. Zanjanchi. Photoactive behavior of polyacrylonitrile fibers based on silver and zirconium co-doped titania nanocomposites: Synthesis, characterization, and comparative study of solid-phase photocatalytic self-cleaning. J. Appl. Polym. Sci., 2013, 3778–3789.

[289] P. Benjwal, K. K. Kar. Removal of methylene blue from wastewater under a low power irradiation source by Zn, Mn co-doped TiO_2 photocatalysts. RSC Adv., 2015, 5, 98166–98176.

[290] K. C. Christoforidis, M. Fernández-García. Photoactivity and charge trapping sites in copper and vanadium doped anatase TiO_2 nano-materials. Catal. Sci. Technol., 2016, 6, 1094–1105.

[291] K. B. Jaimy, V. P. Safeena, S. Ghosh, N. Y. Hebalkar, K. G. K. Warrier. Photocatalytic activity enhancement in doped titanium dioxide by crystal defects. Dalton Trans., 2012, 41, 4824–4832.

[292] L. M. Sun, X. Zhao, X. F. Cheng, H. G. Sun, Y. L. Li, P. Li, W. L. Fan. Synergistic effects in La/N codoped TiO_2 anatase (101) surface correlated with enhanced visible-light photocatalytic activity. Langmuir, 2012, 28, 5882–5891.

[293] L. Yu, X. Yang, J. He, Y. He, D. Wang. One-step hydrothermal method to prepare nitrogen and lanthanum co-doped TiO_2 nanocrystals with exposed {001} facets and study on their photocatalytic activities in visible light. J. Alloy Compd., 2015, 637, 308–314.

[294] G. Li, J. Li, G. Li, G. Jiang. N and Ti^{3+} co-doped 3D anatase TiO_2 superstructures composed of ultrathin nanosheets with enhanced visible light photocatalytic activity. J. Mater. Chem. A, 2015, 3, 22073–22080.

[295] E. Wang, T. He, L. Zhao, Y. Chen, Y. Cao. Improved visible light photocatalytic activity of titania doped with tin and nitrogen. J. Mater. Chem., 2011, 21, 144–150.

[296] Y. Hu, G. Chen, C. Li, Y. Yu, J. Sun, H. Dong. Improved light absorption and photocatalytic activity of Zn, N-TiO_{2-x} rich in oxygen vacancies synthesized by nitridation and hydrogenation. N. J. Chem., 2015, 39, 2417–2420.

[297] L. L. Lai, J. M. Wu. A facile solution approach to W, N co-doped TiO_2 nanobelt thin films with high photocatalytic activity. J. Mater. Chem. A, 2015, 3, 15863–15868.

[298] T. Mishra, M. Mahato, Noor Aman, J. N. Patel, R. K. Sahu. A mesoporous WN co-doped titania nanomaterial with enhanced photocatalytic aqueous nitrate removal activity under visible light. Catal. Sci. Technol., 2011, 1, 609–615.

[299] X. Wang, Y. Yan, B. Hao, G. Chen. Biomimetic layer-by-layer deposition assisted synthesis of Cu, N co-doped TiO_2 nanosheets with enhanced visible light photocatalytic performance. Dalton Trans., 2014, 43, 14054–14060.

[300] Y. Zhang, W. Zhu, X. Cui, W. Yao, T. Duan. One-step hydrothermal synthesis of iron and nitrogen co-doped TiO_2 nanotubes with enhanced visible-light photocatalytic activity. CrystEngComm, 2015, 17, 8368–8376.

[301] Q. Liu, D. Ding, C. Ning, X. Wang. Reduced N/Ni-doped TiO_2 nanotubes photoanodes for photoelectrochemical water splitting. RSC Adv., 2015, 5, 95478–95487.

[302] J. Zhang, X. Wang, X. Wang, J. Song, J. Huang, B. Louangsouphom, J. Zhao. Floating photocatalysts based on loading Bi/N-doped TiO_2 on expanded graphite C/C (EGC) composites for the visible light degradation of Diesel. RSC Adv., 2015, 5, 71922–71931.

[303] J. Xu, C. Chen, X. Xiao, L. Liao, L. Miao, W. Wu, F. Mei, A. L. Stepanov, G. Cai, Y. Liu, Z. Dai, F. Ren, C. Jiang, J. Liu. Synergistic effect of V/N codoping by ion implantation on the electronic and optical properties of TiO_2. J. Appl. Phys., 2014, 115(14), 143106.

[304] J. Zhang, J. Xi, Z. Ji. (Mo, N)-codoped TiO_2 sheets with dominant {001} facets for enhancing visible-light photocatalytic activity. J. Mater. Chem., 2012, 22, 17700–17708.

[305] W. He, Z. Fang, K. Zhang, X. Li, D. Ji, X. Jiang, C. Qiu, K. Guo. Continuous synthesis of a co-doped TiO_2 photocatalyst and its enhanced visible light catalytic activity using a photocatalysis microreactor. RSC Adv., 2015, 5, 54853–54860.

[306] Y. Zhang, H. Zhang, L. Cheng, Y. Miao, L. Hu, G. Ding, Z. Jiao, L. Bian, M. Nguyen, G. Zheng. Vacuum-treated Mo, S-doped TiO_2:Gd mesoporous nanospheres: An improved visible-light photocatalyst. Eur. J. Inorg. Chem., 2015, 2895–2900.

[307] C. Yan, W. Yi, H. Yuan, X. Wu, F. Li. A highly photoactive S, Cu-codoped nano-TiO_2 photocatalyst: Synthesis and characterization for enhanced photocatalytic degradation of neutral red. Environ. Prog. Sustain. Energ., 2014, 33(2), 419–429.

[308] W. Fu, S. Ding, Y. Wang, L. Wu, D. Zhang, Z. Pan, R. Wang, Z. Zhang, S. Qiu. F, Ca co-doped TiO_2 nanocrystals with enhanced photocatalytic activity. Dalton Trans., 2014, 43, 16160–16163.

[309] R. Jaiswal, N. Patel, A. Dashora, R. Fernandes, M. Yadav, R. Edla, R. S. Varma, D. C. Kothari, B. L. Ahuja, A. Miotello. Efficient Co-B-codoped TiO_2 photocatalyst for degradation of organic water pollutant under visible light. Appl. Catal. B Environ., 2016, 183, 242–253.

[310] R. Li, G. Dong, G. Chen. Synthesis, characterization and performance of ternary doped Cu-Ce-B/TiO_2 nanotubes on the photocatalytic removal of nitrogen oxides. N. J. Chem., 2015, 39, 6854–6863.

[311] J. M. Wu, M. L. Tang. One-pot synthesis of N-F-Cr-doped anatase TiO_2 microspheres with nearly all-(001) surface for enhanced solar absorption. Nanoscale, 2011, 3, 3915–3922.